Click here to view linked References

Rational design of Nd_2O_3 decorated functionalized carbon nanofiber composite for selective electrochemical detection of carbendazim fungicides in vegetables, water, and soil samples

Selvakumar Palanisamy[a#*], Krishnapandi Alagumalai[b#], Matteo Chiesa[a, c*], Seong-Cheol Kim[b*].

[a]Laboratory for Energy and NanoScience (LENS), Khalifa University of Science and Technology, Masdar Campus, PO Box, 54224, Abu Dhabi, United Arab Emirates.

[b]School of Chemical Engineering, Yeungnam University, Gyeongsan 38541, Republic of Korea.

[c]Department of Physics and Technology, UiT The Artic University of Norway, 9010, Tromso, Norway.

[#]These authors contributed equally.

[*]Corresponding Authors

Selvakumar Palanisamy: prmselva@gmail.com

Matteo Chiesa: Email: matteo.chiesa@ku.ac.ae

Seong-Cheol Kim: Email: sckim07@ynu.ac.kr

Abstract

Abuse of carbendazim (CBZ) leaves excessive pesticide residues on agricultural products, which endangers human health because of the residues' high concentrations. Hence, a composite consisting of functionalized carbon nanofibers (*f*-CNF) with neodymium oxide (Nd_2O_3) was fabricated to monitor CBZ at trace levels. The Nd_2O_3/*f*-CNF composite-modified electrode displays higher electro-oxidation ability towards CBZ than Nd_2O_3 and *f*-CNF-modified electrodes. The combined unique properties of Nd_2O_3 and *f*-CNF result in a substantial specific surface area, superior structural stability, and excellent electrocatalytic activity of the composite yielding enhanced sensitivity to detecting CBZ with a detection limit of 4.3 nM. Also, the fabricated sensor electrode can detect CBZ in the linear concentration range of up to 243.0 µM with high selectivity, appropriate reproducibility, and stability. A demonstration of the sensing capability of CBZ in vegetables, water, and soil samples was reported paving the way for its use in practical applications.

Keywords: Fungicides detecting sensor; Carbendazim; Nd_2O_3; Functionalized carbon nanofibers composite; Electroanalysis

1. Introduction

Fungicides are frequently employed in modern agriculture to safeguard crops against fungi and boost yields [1,2]. Pesticide residues in the environment pose a severe risk to ecological safety, human health, food quality, and water supply [3]. Carbendazim (Methyl-2-benzimidazole carbamate, CBZ) is extensively used for crop protection and fast growth in the cultivation of various fruits and vegetables [4,5]. It can be utilized for pre-planting and post-harvesting in addition to seed storage before and after harvest [6,7]. However, prolonged or excessive exposure to CBZ can seriously damage soils, leading to contaminated groundwater and adverse effects on people and animals [8]. The benzimidazole ring attached to the structure of CBZ is responsible for the long-term stability and half-life of the compound (>3 years) [9]. Despite being banned in many countries, it is still used for plant cultivation because of its low cost and ability to accelerate growth [10]. Also, CBZ has been classified as a probable human carcinogen by the World Health Organization (WHO), and the multiplication of pesticide residues can cause severe adverse effects in humans and aquatic animals, including allergic reactions, dermatitis, eye irritation, hormonal abnormalities, infertility, teratogenicity, and mutagenicity [11,12]. This highlights the importance of concentrating on the quantitative development of efficient CBZ residue detection technologies. For identifying CBZ in various water sources, various cutting-edge analytical methods are available, including chemiluminescence, high-performance liquid chromatography, Raman scattering, UV-Vis spectrometry, and electrochemical detection [13,14,15]. Traditional chromatographic and spectroscopic techniques are sensitive, but they have certain drawbacks, such as the need for complex instrumentation, incapability for real-time observation, and length of time [16]. Electrochemical sensors have gained significant attention among other techniques because they are easy to use, high-accurate, inexpensive, quick, and use minimal chemicals [17].

Consequently, our approach to identifying CBZ in food samples was based on electrochemical methods.

The distinctive qualities of rare-earth metal oxides (La_2O_3, CeO_2, Pr_6O_{11}, and Nd_2O_3), such as electron richness in the d and f orbitals, catalytic effectiveness, optical, magnetic, and thermal stability, are what make them so popular for a variety of applications [18,19]. Among the lanthanide family, neodymium oxide (Nd_2O_3) is a more reactive oxide found naturally over most of the earth's crust. Also, Nd_2O_3 has been widely used in solar cells, lithium-ion batteries, supercapacitors, and sensors due to its improved catalytic and electric properties [23,24]. To date, various synthesis methods have been used to synthesize Nd_2O_3, including hydrothermal synthesis, sol-gel auto combustion, template synthesis, polyol synthesis, microemulsion synthesis, inductively coupled radiofrequency thermal plasma, and micro-aided synthesis [25-27]. Nevertheless, the improvements on single metal oxides still suffer from poor applicability, low conductivity, and unsatisfactory cyclic stability during the chemical reaction [28]. Therefore, developing a carbon matrix that can be modified efficiently to enhance the electrocatalyst for environmental hazards sensors is imperative [29,30]. Our previous study revealed that lanthanide oxides with functionalized carbon nanofibers (*f*-CNF) could selectively detect CBZ with improved sensitivity [31]. The surface properties of *f*-CNF are similar to those of other carbon nanomaterials (graphene oxide and functionalized carbon nanotubes), which makes it suitable for electrochemical sensor applications [32-34]. Furthermore, *f*-CNF has many free hydroxyl groups on its cylindrical surface, which makes it an ideal material to disperse in an aqueous solution. [35]. As a result of its unique surface properties and cylindrical nanostructure nature, *f*-CNF would significantly boost the electron conductivity and electrochemical performance of lanthanide oxides [31]. According to a literature survey, *f*-CNF-based composite materials have been used for the electrochemical determination of various analytes, including CBZ [31-40]. As far as we know, there is no report on the detection of CBZ utilizing Nd_2O_3 with *f*-CNF nanocomposite. The Nd_2O_3/*f*-CNF modified electrode was employed for the sensitive and lower potential detection of CBZ by cyclic voltammetry (CV) and differential pulse voltammetry (DPV) for electrochemical sensor applications. The fabricated sensor displayed a more comprehensive linear range, a lower detection threshold, and good sensitivity. Additionally, it demonstrated respectable applicability for examining CBZ in real samples, such as beet, carrot, and cabbage.

2. Experimental section

2.1. Materials and reagents

Neodymium (III) chloride (99.9% trace metals basis), ethylene glycol, Urea, malathion, parathion, thiamethoxam, carbofuran, ascorbic acid, caffeic acid, and carbendazim were purchased from Sigma-Aldrich and used without any further purification. Carbon nanofibers (98% amorphous carbon with iron impurities below 14000 ppm, diameter =100 mm, length = 20-200 µm, and surface area 39 m^2/g) were purchased from Sigma-Aldrich. Monosodium phosphate (≥99%) and disodium phosphate (≥98.5%) were used to make different concentrations supporting electrolyte solution during electrochemical analysis, and HCl and NaOH were used to adjust the pH value. All other chemicals used in this study were purchased from Sigma-Aldrich and used as received.

2.2. Synthesis and fabrication of Nd_2O_3/*f*-CNF modified electrode

The Nd_2O_3 was synthesized via a cost-effective familiar coprecipitation method. In general, 0.1 M of Nd $(NO_3)_3.6H_2O$ was dissolved in 40 mL of deionized (DI) water and allowed to continue stirring at room temperature. About 10.0 mL of ethylene glycol was added slowly into the above mixture and stirred for 90 minutes at 4000 RPM. A white and homogeneous precipitate was obtained at the end of the reaction. The reaction mixture in the beaker was kept under an ultrasonication bath for 1 h for homogeneous formation. The settled residue was washed with DI water and ethanol 3 times before centrifuging at 4000 rpm to remove external impurities. Afterward, the obtained precipitates were dehydrated at 55 ºC for 24 h. The synthesized product (Nd_2O_3) was calcined at 500 ºC for 6 h and used for further characterization. The *f*-CNF was synthesized using an acid functionalization method reported early [31].

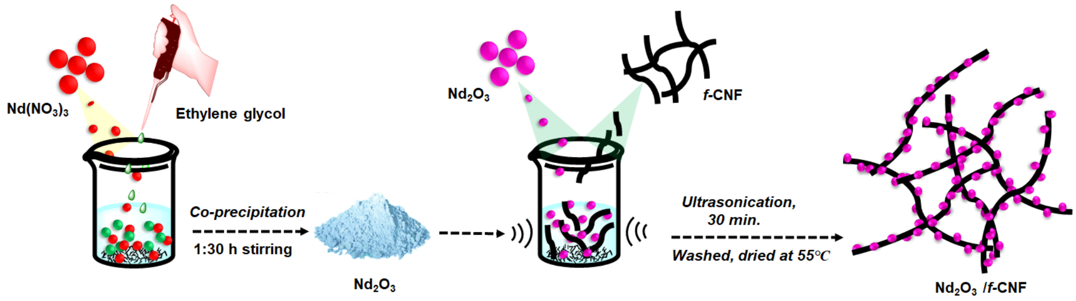

Scheme 1. A schematic representation of the overall synthesis process of Nd_2O_3/*f*-CNF composite.

As preparation for the electrocatalyst, 8 mg of Nd_2O_3 and 4 mg *f*-CNF were added to the vial containing DI water. The mixture was kept under the ultrasonic bath and sonicated until a homogenous suspension was obtained. Afterward, the suspension was centrifuged at 4000 rpm for 15 minutes and washed numerous times with DI water and ethanol to remove impurities. The obtained Nd_2O_3/f-CNF was dried at 80 °C for 8 h. Oxidized carboxylic functional groups in *f*-CNF allow the Nd_2O_3 nanoparticles to adhere well to the outer interlayers of the structure during ultrasonication. A schematic representation of the overall synthesis process of the Nd_2O_3/*f*-CNF composite is shown in **Scheme 1**. We prepared the Nd_2O_3/*f*-CNF composite dispersion by ultrasonically dispersing 3 mg of the composite in 1 mL of DI water for 15 minutes at room temperature. After that, the Nd_2O_3/*f*-CNF composite dispersion was drop cast (6 µL) over the glassy carbon electrode (GCE) surface, and the suspension was allowed to dry at ambient temperature. The fabricated Nd_2O_3/*f*-CNF composite electrode was further used for the electrochemical/catalytic studies, and the same electrode preparation procedure was used for all experiments.

2.3. Apparatus and measurements

Powder X-ray diffraction (XRD) patterns of synthesized Nd_2O_3, *f*-CNF, and Nd_2O_3/*f*-CNF composite were studied using a PAN analytical X'Pert PRO diffractometer with Cu Kα radiation (λ = 1.5418 Å). Each sample's crystal structure was investigated in the 10-90° 2θ with a 0.02° step size. IR spectrum of the synthesized samples was recorded using a KBr disc on a JASCO Fourier transform infrared (FT-IR) 460 Plus spectrophotometer. A Raman spectrometer with a charge-coupled detector (Dong Woo 500i, Korea) was used to investigate particle size, morphology, and vibration modes. X-ray photoelectron spectroscopy (XPS) analyzed the prepared samples' elemental composition and oxidation state (XPS, Thermo Scientific Multi-Lab 2000). A High-Resolution Transmission Electron Microscope (HR-TEM): JEOL 2100F was used for scanning images, selected area electron diffraction (SEAD), and elemental mapping. The pH of the sample was measured with a Horiba-L aqua pH meter calibrated with a standard buffer of the relevant pH.

The electrochemical experiments were carried out using a conventional three-electrode system equipped with a modified GCE as a working electrode, a platinum wire as an auxiliary electrode, and Ag/AgCl (sat.KCl) as a reference electrode. Alumina-silica powder was used to clean all electrodes before beginning electrochemical experiments. A CHI 750A electrochemical workstation (CH Instruments, USA) was used for the electrochemical studies, including CV and DPV experiments.

3. Results and Discussion

3.1. Characterization

The HR-TEM was used to analyze the surface morphology of as-synthesized *f*-CNF, Nd_2O_3, and Nd_2O_3/*f*-CNF composite. In **Fig.1A**, the TEM image of the *f*-CNF clearly shows stacked-cup carbon nanofibers, which are visible in the magnified image. It was calculated that the average diameter and width of the *f*-CNF are 226 nm and 142 nm, respectively. In **Fig.1B** and **C**, the sphere-like structure of the Nd_2O_3 nanoparticles can be seen with a uniform size of around 80-100 nm with a diameter of 160-200 nm. A TEM image of the Nd_2O_3/*f*-CNF composite (D-E) revealed successful embattlement of Nd_2O_3 nanoparticles on the surface of *f*-CNF. Also, the Nd_2O_3 nanoparticles were evenly attached with slight aggregation (**Fig.1F**).

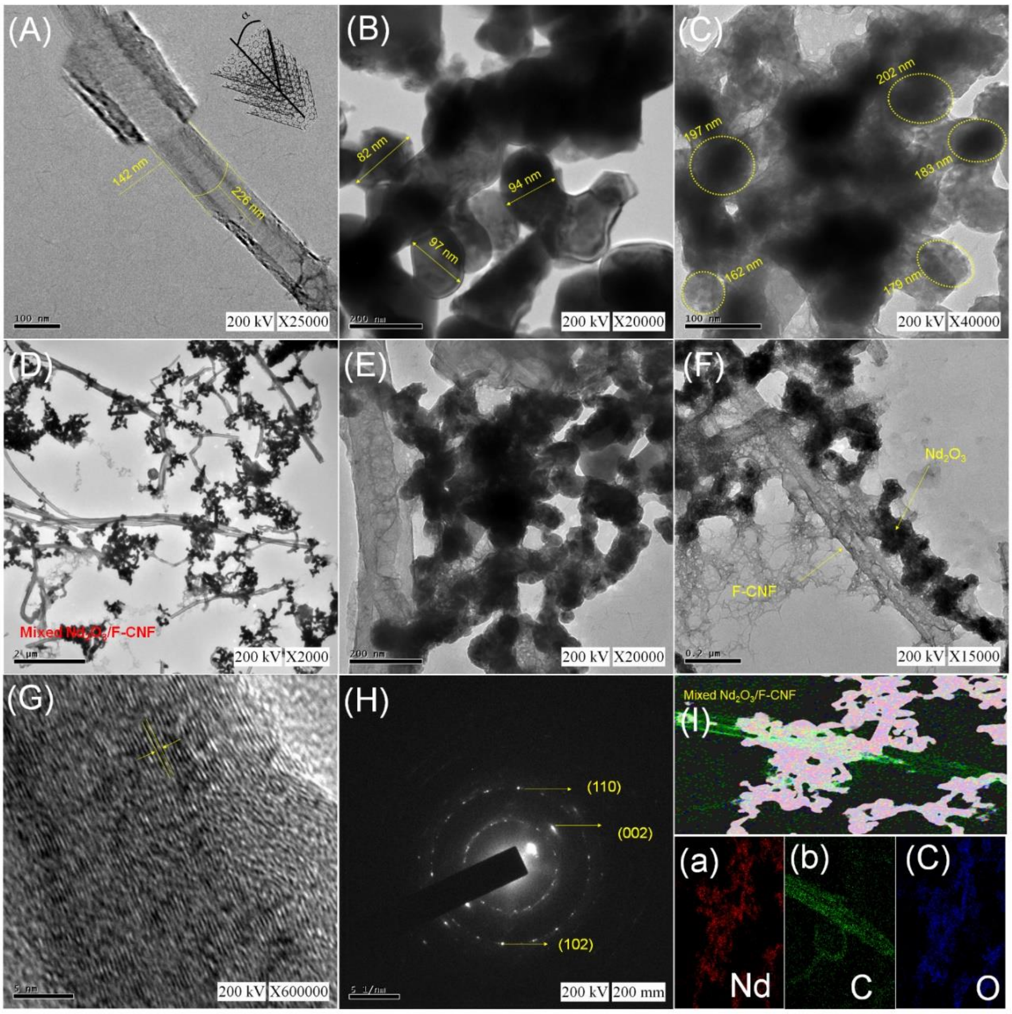

Figure 1. HR-TEM images of (A) *f*-CNF, (B, C) Nd_2O_3, and Nd_2O_3/*f*-CNF composite in different magnifications (D-F), Lattice fringe for Nd_2O_3 (G). SEAD pattern of Nd_2O_3, and elemental mapping of Nd, C, and O for Nd_2O_3/*f*-CNF composite.

The (111) plane of the *f*-CNF was attributed to the lattice fringe distance of 0.21 nm, and a well-resolved Nd_2O_3 crystal ring pattern was observed in **Fig. 1G**, whose ring spots matched XRD plane values including (110), (002), and (102) (**Fig. 1H**). The results confirmed that the high crystal nature of Nd_2O_3 was unaffected by *f*-CNF in the Nd_2O_3/*f*-CNF composite. In **Fig. 1I**, we see that the Nd (a), O (b), and C (c) are evenly distributed throughout the Nd_2O_3/f-CNF composite, indicating that the fabrication was successful and uninterrupted.

Fig. 2A of the Raman spectra of Nd_2O_3 show the lower and higher number bands at 90.1, 121, 133.5, 195.3, 338.4, 431.6, 546.5, and 1009.2, 1077.3, 1356.7, 1611.2, 1927 cm^{-1}, which relate to Fg and Ag + Eg modes, respectively [41]. The Raman spectra of the *f*-CNF show that the D and G bands at 1348 and 1589 cm^{-1} result from disordered and ordered graphitic carbon on CNF [26]. In contrast, the decrease in G-band intensity indicates a low level of impurities and high crystallinity of CNF. In addition, the graphitic carbon (G band) and carbon (D band) of the *f*-CNF are arranged orderly, which means that no defects are observed in the *f*-CNF. The contrast between the *f*-CNF and Nd_2O_3, the Nd_2O_3/*f*-CNF composite peak intensity indicates disorder in the sp^2 carbon lattice and compressive strains induced by the bonds between *f*-CNF and oxygen adsorption on surfaces of transition metal oxides. FTIR spectroscopy was used to identify the functional groups in Nd_2O_3 nanoparticles, *f*-CNF, and Nd_2O_3/*f*-CNF nanocomposite. As shown in **Fig. 2B**, the broad peak at 3490 - 3600 cm^{-1} corresponds to the -OH stretching vibration, while the broad blend peak at 1639 cm^{-1} is attributed to the CO stretching vibration. The two significant peaks at 566 cm^{-1} and 725 cm^{-1} are related to the Nd-O stretching vibration (metal-oxygen bond), showing the formation of Nd_2O_3 nanoparticles [25]. Three other series peaks between 1030 and 1232 cm^{-1} are associated with the stretching vibration of the carbon and hydroxyl group (C-OH) bond. The broader peaks 1048 and 1526 cm^{-1} are according to the asymmetric and symmetric vibrations of the O-C-O bond. FTIR spectrum of *f*-CNF revealed the following peaks at 1225.7, 1538.8, 1646, 1701, and 3462 cm^{-1}, which correspond to the acid-treated functional groups C-O, C=C, C-O-C, C=O, and -OH [42]. This was similar to the peak observed in the Nd_2O_3/*f*-CNF composite, which confirmed the presence of *f*-CNF and Nd_2O_3. Also, the Raman spectra of *f*-CNF exhibited two distinct peaks at 1362 cm^{-1} and 1606 cm^{-1}, which are attributed to the D band and G band, indicating the successful formation of *f*-CNF. An XRD analysis was performed to determine the phase purity and crystal structure of the as-synthesized Nd_2O_3, *f*-CNF, and Nd_2O_3/*f*-CNF composites.

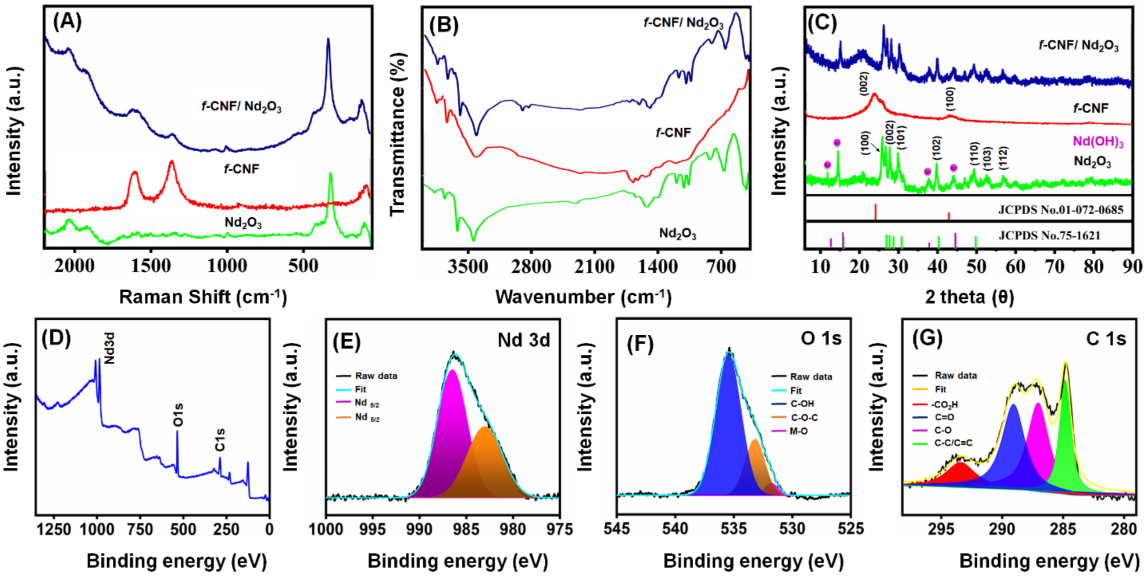

Figure 2. A) Raman, (B) FTIR and C) XRD spectra of *f*-CNF, Nd_2O_3, and Nd_2O_3/*f*-CNF composite, D) Survey spectra of Nd_2O_3/*f*-CNF composite and (E-G) individual XPS spectra of Nd 3d, C 1s, and O 1s.

Fig. 2C displays the XRD pattern of Nd_2O_3. As visible in **Fig. 2C**, the diffraction peaks at 2θ of 27.0°, 28.8°, 30.8°, 40.4°, 49.6°, 52.9°, and 57.1° are associated with hexagonal phases (100), (002), (101), (102), (110), (103), and (112) and are well-matched with the previously reported literature [JCPDS:00-43-102] [28]. Using Debye-Scherrer's equation (1), we calculated the average crystalline size of Nd_2O_3.

$$D_{XRD} = {}^{K\lambda}/_{\beta_{hkl} COS\theta} \qquad (1)$$

Where λ is the wavelength of X-ray (0.15406 Å), D represents the size of crystallites (nm), q is the diffraction angle, k is a constant value, and β is full with half maximum (FWHM) of the diffraction peak. The calculated average crystalline size (D) of the Nd_2O_3 was 63.1 nm. The results show that the synthesized Nd_2O_3 consists only of Nd, O, and no other impurities. Several other peaks were also observed at 13.2°, 15.7°, 38.3°, and 42.6°, which correspond to the hexagonal structure of $Nd(OH)_3$. According to the XRD pattern of the *f*-CNF, the peaks at 24.4° and 42.2° were well indexed with (002) and (100), respectively, indicating the presence of a carbon source [35]. The presence of *f*-CNF partially influenced Nd_2O_3, and accordingly, some combinations disappeared because of *f*-CNF. Additionally, XPS spectra of Nd_2O_3/f-CNF nanocomposite revealed its chemical composition and oxidation state. As shown in **Fig. 2D**, the Nd_2O_3/*f*-CNF composite spectra are located at 985.5, 355.6, and 286.9eV, indicating the presence of Nd 3d, O1s, and C 1s. **Fig. 2D** shows the Nd 3d XPS spectrum of Nd_2O_3 at 986.3 eV, which is further deconvoluted into two Nd^{3+} peaks at 982.3 eV and 986.1 eV corresponding to Nd $3d_{5/2}$. In **Fig. 2F**, the O1s peaks correspond to the aromatic C-OH, C-O-C, and M-O bonds (metal-oxygen bonds). Also, the C 1s spectrum of **Fig. 2G** show four different oxygen peaks at binding energies of 294.1, 289.4, 286.8, and 285.1; these correspond to functional groups such as $-CO_2H$, C=O, C-O, and Sp^3/Sp^2 orbital bonds in the surface of the Nd_2O_3/*f*-CNF composite [36]. The above results confirmed the successful formation of Nd_2O_3/*f*-CNF nanocomposite.

3.2. Electrochemical and catalytic properties of the modified electrode

The electron transfer and electroactive surface area of different electrodes were determined using CV. A mixed solution of 0.5 M $Fe(CN)_6^{3-/4-}$ and 0.1 M KCl was used to test the electrochemical performance of the modified and unmodified electrodes. According to **Fig. 3A**, the bare GCE displays a weak redox peak response due to a low electron transfer rate. After GCE was modified with Nd_2O_3, *f*-CNF, and Nd_2O_3/*f*-CNF, the redox peak current of GCE gradually increased. From these experiments, Nd_2O_3/*f*-CNF/GCE show a higher redox peak current than other electrodes, possibly because the Nd_2O_3 interacts with the surface-etched f-CNF with a strong π-π bond, which can result in improved electrocatalytic activity and electron transfer kinetics in Nd_2O_3/*f*-CNF/GCE.

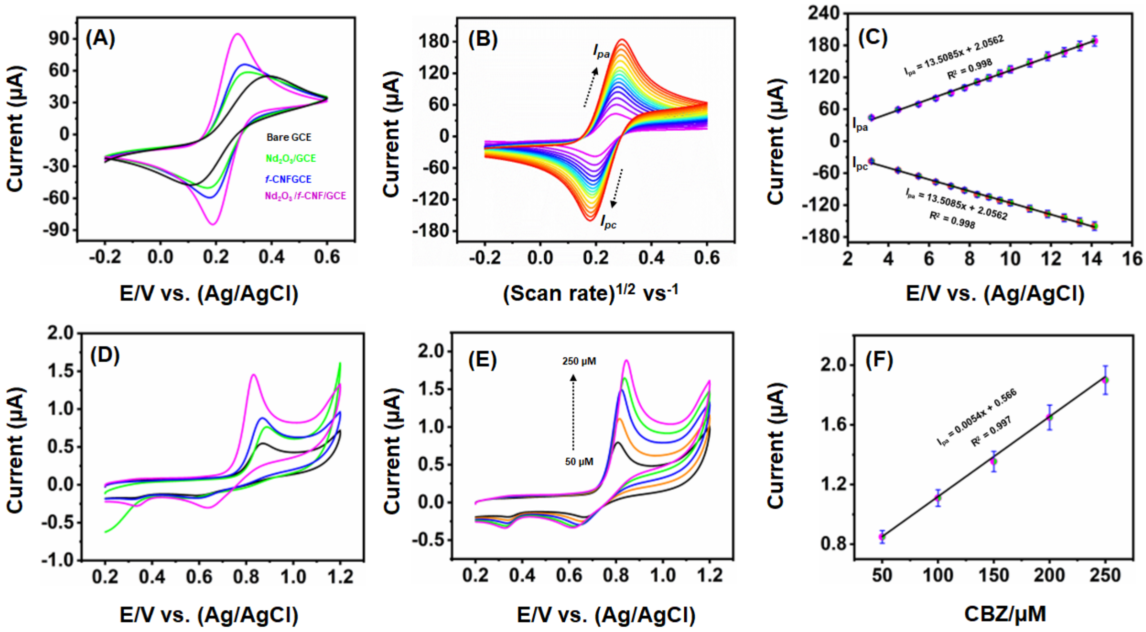

Figure 3. A) CV response of bare GCE, Nd_2O_3/GCE, *f*-CNF/GCE, and Nd_2O_3/*f*-CNF/GCE in 0.5 M of $[Fe(CN)_6]^{3-/4-}$ comprises 0.1 M of KCl at a scan rate of 50 mV s^{-1}. B) At the same conditions, the CV response of Nd_2O_3/*f*-CNF/GCE at different scan rates from 10 to 200 mV s^{-1}. C) The linear relationship between the square root of scan rate (mV s^{-1}) *vs.* anodic and cathodic peak current (I_{pa} and I_{pc}) response. D) CV curves of different electrodes at scan rate 50 mVs^{-1} in the presence of 100 µM CBZ in PH 7.0. The color description for the different electrodes is the same as in (A). E) CV response for adding different quantities of CBZ (50-250 µM) on Nd_2O_3/*f*-CNF/GCE in pH 7.0 at a scan rate of 50 mV s^{-1}. F) The linear relationship between the [CBZ] *vs.* I_{pa}.

We also measured the electroactive surface area of the unmodified and modified electrodes in a mixed solution of 0.5 M $Fe(CN)_6^{3-/4-}$ and 0.1 M KCl solution at various scan rates from 10 to 200 mV s^{-1} (**Fig. 3B**). The results confirmed that the square root of scan rates had linear dependence with the anodic and cathodic peak current response of the Ferro/Ferri redox couple (**Fig. 3C**). Electroactive surface area of various modified GCEs were calculated using Randles–Ševćik equation for reversible electrochemical processes [**43**]. Using the Rendles-Sevick equation (2), the active surface areas of the Nd_2O_3/GCE, *f*-CNF/GCE, and Nd_2O_3/*f*-CNF/GCE were calculated to be 0.079, 0.088, and 0.094 cm^{-2}, respectively.

$$I^{rev} = 0.446\, n\, FA_{real}\, C\, \sqrt{\frac{nFDv}{RT}} \ldots\ldots\ldots\ldots\ldots\ldots\ldots\ldots\ldots\ldots (2)$$

Where I^{rev} is the redox peak current (µA), *A* is the electroactive surface area (cm^2), A is the surface area of the electrode, C is the concentration, *D* is the diffusion coefficient (7.6 x 10^{-6}), and *n* is the number of electrons (n=1), and *v* is scan rate (Vs^{-1}). Also, the % of real and geometrical surface area of bare GCE was calculated using %real = (A_{real}/A_{geo}) × 100). The % of real was 86.1% when compared to the active surface area of 0.068 cm^2. The above results make clear that the Nd_2O_3/*f*-

CNF/GCE has a higher electroactive surface area among the other electrodes and can be used for the enhanced electrochemical detection of CBZ.

The electrochemical response of different electrodes was examined by CV with 100 µM CBZ in 0.1 M PBS (pH 7.0) at a scanning rate of 50 mVs^{-1} with the potential scanning from 0.3 to 1.3 V. The color description for the different electrodes is the same as in **Fig. 3A**. As shown in **Fig. 3D**, the bare GCE exhibits a low oxidation peak current of 0.61 µA response with the higher oxidation potential (E_{pa}) due to low electron transfer kinetics and poor catalytic performance. The peak current and peak potential of modified electrodes gradually increased, as shown in **Fig. 3D**, Nd_2O_3/GCE (I_{pa} = 0.75 µA, E_{pa} = 0.839 V)> *f*-CNF/GCE (I_{pa} = 0.85 µA, E_{pa} = 0.816 V)> Nd_2O_3/*f*-CNF/GCE (I_{pa} = 1.5 µA, E_{pa} = 0.8 V). Compared with other electrodes, the Nd_2O_3/*f*-CNF/GCE exhibited a higher oxidation peak current response and a lower oxidation peak potential, indicating that the Nd_2O_3/*f*-CNF composite modified electrode can be used for sensitive and lower potential detection of CBZ. The combined unique properties of *f*-CNF and Nd_2O_3 through π-π interactions had a synergistic effect on enhancing the electrocatalytic activity against CBZ oxidation. The anodic peak in carbendazim comes from the oxidation of nitrogen atoms in the pyridine ring of benzimidazole. The possible oxidation mechanism of CBZ on the Nd_2O_3/*f*-CNF composite-modified electrode is elucidated in **Scheme 2** [31].

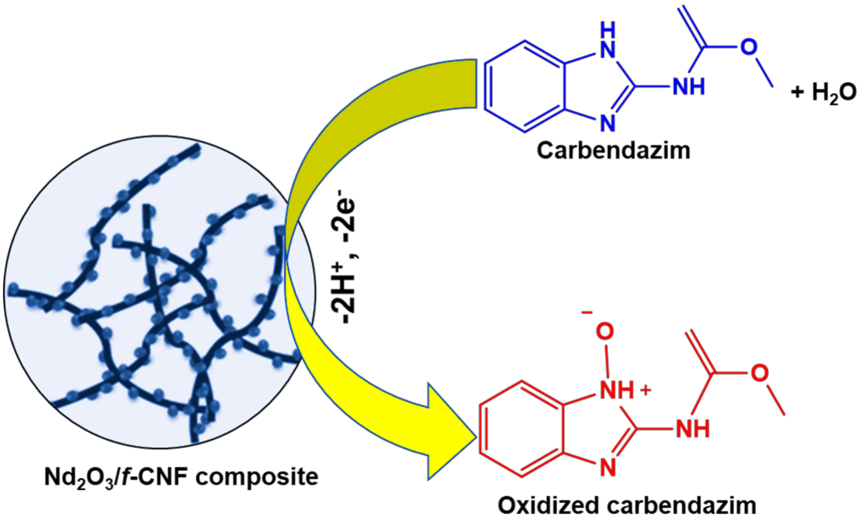

Scheme 2 Possible electrochemical oxidation mechanism of CBZ on Nd_2O_3/*f*-CNF composite modified electrode.

A quantitative assessment of CBZ was performed by CV at various concentrations (50-250 µM) in 0.1 M PBS at 50 mVs^{-1} (**Fig. 3E**). As concentrations of CBZ increased linearly, their peak currents also increased, and their potential shifted slightly from its original potential. As shown in **Fig. 3F**, the linear regression equation for the oxidation peak current is $I_{pa} = 0.0054[CPZ] + 0.566$ ($R^2 = 0.991$). The results indicate the excellent kinetics and higher electrocatalytic activity of Nd_2O_3/*f*-CNF/GCE towards CBZ.

3.3. Influence of scan rate and pH

We examined the impact of various scan rates on CBZ detection at Nd_2O_3/*f*-CNF/GCE in 0.1 M PBS (pH 7.0) containing CBZ (100 µM), as shown in **Fig. 4A**. As the scan rate increased, the oxidation peak current of CBZ also increased, and the peak current in the potential range was proportional to the scan rate obtained. This was described using the equation $I_{pa} = 0.0085v + 0.3169$ (R2=0.994) as the relationship plot between scan rates (mVs^{-1}) vs. I_{pa}. Further, the linear relationship between reduction peak current vs. scan rate (mVs^{-1}) is $I_{pc} = 0.1647v + 0.3889$ ($R^2 = 0.96$). The result implies that the electrochemical reaction of CBZ on the Nd_2O_3/*f*-CNF/GCE is the surface adsorption-controlled electrochemical reaction [31]. We examined the effect of pH for CBZ sensing (100 µM) at Nd_2O_3/*f*-CNF/GCE by using different pH (3.0 - 11.0) at a scan rate of 50 mV s^{-1} (**Fig. 4C**). By varying the pH of an electrolyte containing CBZ from low to high, the peak current and potential have moved towards the negative range, suggesting that protons are involved in the electrode reaction. In this study, pH 7.0 was determined to be the optimal pH value based on the maximum oxidation current observed. It was found that E_{pa} (V) = -0.0715 pH + 1.3115 ($R^2 = 0.998$) for different pH versus E_{pa} (V), which indicates the linear dependence of E_{pa} in a broader pH range.

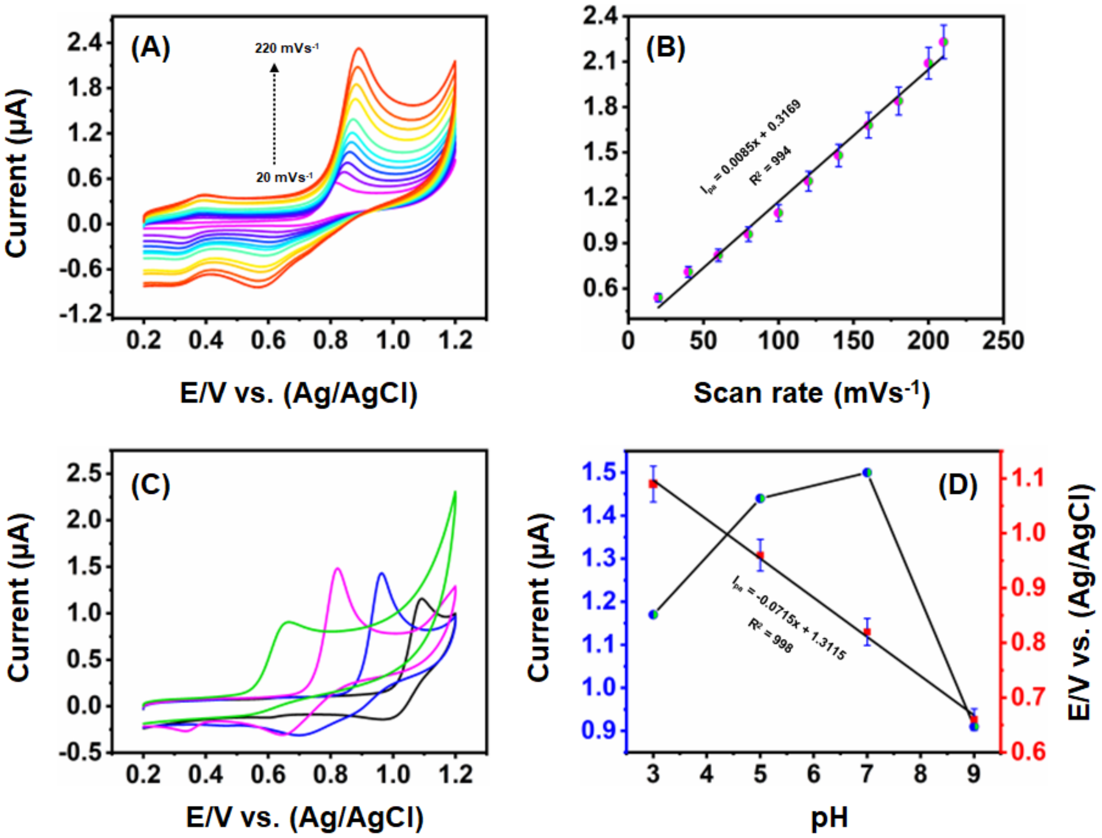

Fig. 4. A) CV response for CBZ (200 μM) at Nd_2O_3/*f*-CNF/GCE with different scan rates (20–220 mVs^{-1}). B) The linear relationship between the different scan rates *vs.* I_{pa}. C) CV response at Nd_2O_3/*f*-CNF/GCE with 100 μM CBZ containing different pH (pH 3.0–7.0) at scan rate 50 mVs^{-1}. D) The linear relationship between the pH *vs.* I_{pa} and E_{pa}.

3.4. Determination of CBZ at Nd_2O_3/*f*-CNF/GCE

In contrast to other electrochemical approaches, DPV has a higher detection sensitivity and a lower detection limit, making it an ideal technique for determining CBZ. **Fig. 5A** shows the DPV response current of CBZ at the Nd_2O_3/*f*-CNF/GCE for different concentration addition of CBZ, ranging from 0.1 to 243 μM. Under optimized conditions, the response current of CBZ shows a significantly enhanced trend upon increasing the CBZ concentration from 0.1 to 243 μM.

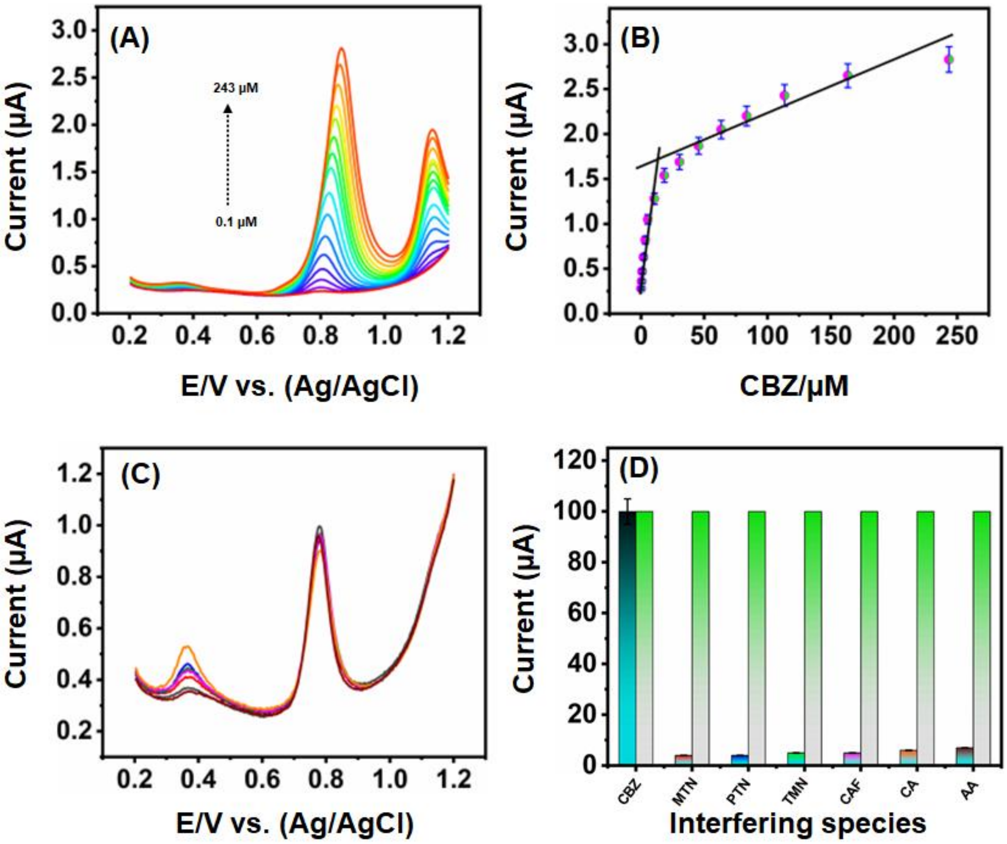

Figure 5. A) DPV curves of the Nd_2O_3/*f*-CNF/GCE for the successive addition of CBZ from 0.1 to 243 μM in pH 7.0. B) The linear relationship between the [CBZ] *vs.* I_{pa}. C) Selectivity of the sensor in the presence of co-inferring species and its corresponding error bar diagram (D).

Based on the DPV results, two linear curves are plotted at low and high CBZ concentrations. According to the first linear equation, I_{pa} (A) = 0.142 *C*[CBZ] +0.3152 (R^2 = 0.984) in the concentration range of 0.1-5.4 μM for CBZ. In the CBZ concentration range of 10.4-243 μM, the second equation is expressed as I_{pa} (A) = 0.0064 *C*[CBZ] + 1.5114 (R^2 = 0.895). Due to the empty free active sites on the electrode surface, CBZ is rapidly adsorbed on the electrode surface when injected consecutively. With high concentration, the CBZ curves shifted toward a more positive region with a low oxidation current. Also, the oxidation of CBZ at modified Nd_2O_3/*f*-

CNF composite surfaces is slightly slower because there are fewer unoccupied active sides. Since the occupied sites revealed low electroactive area and sensitivity, the first linear equation was used to calculate the sensor's low detection limit (LOD) and sensitivity. The calculated LOD is 4.3 nM (3Sd/N, where Sd is the standard deviation of blank and N is the slope of the calibration plot) and the analytical sensitivity are 0.142 µA μM^{-1} (slope of the calibration plot). The LOD of the sensor (100 nM) is lower than the WHO-recommended value for water samples. The fabricated sensor's analytical performance was compared with previously reported CBZ sensors to confirm the developed sensor's novelty. Comparative results between the Nd_2O_3/*f*-CNF/GCE sensor and those previously reported in the literature are shown in **Table 1**. Notably, the Nd_2O_3/*f*-CNF/GCE has lower LOD (4.3 nM) than previously used CBZ sensors based on the composites of single and multiwalled carbon nanotubes ($ZnFe_2O_4$/SWCNT and SiO_2/MWCNT), phosphorus-doped helical carbon nanofibers (HCNFs), reduced graphene oxide composites (NP-Cu/RGO and QD-rGO). Also, the sensitivity and linear response of the fabricated sensor is enhanced and comparable to the previously reported CBZ sensors listed in **Table 1**. Therefore, the Nd_2O_3/*f*-CNF composite-modified electrode is a promising alternative electrode material for sensitive and low levels detection of CBZ in environmental samples.

Table 1 Analytical comparison of Nd_2O_3/*f*-CNF composite modified electrode with previously reported modified electrodes for the determination of CBZ.

Electrode	**Linear range (µM)**	**Limit of detection (nM)**	**Sensitivity (µA/µM)**	**Refs.**
La-Nd_2O_3/CPE	0.08-50	27	NR	[21]
Yb_2O_3/f-CNF/GCE	0.05 to 3035	6	0.049	[31]
$ZnFe_2O_4$/SWCNT/GCE	0.5-100	90	NR	[45]
SiO_2/MWCNT/GCE	0.2-4.0	56	0.485	[46]
Ti_3C_2TxMXene/GCE	0.05-100	10.3	NR	[47]
P-HCNFs/GCE	1-35	38	0.92	[48]
NP-Cu/RGO/GCE	0.5-30	90	0.085	[49]
D-PC/GCE	0.01-1.00	6	NR	[50]
Ce-dope $ZnWO_4$/GCE	0.01-5.5	3	0.0289	[51]
$WO_{3.0}$.33H_2/GCE	0.1-250	22	NR	[52]
Fe-CuV/GCE	0.01-83.1	5	0.86	[53]
MBC@CTS/GCE	0.1-20	20	NR	[54]
TCP/CPE	0.5-10	300	0.59	[55]
MWCNTs/GCE	0.256-3.11	54.9	NR	[56]
Nd_2O_3/*f*-CNF/GCE	0.1-243	4.3	0.142	**This work**

NR – Not reported

3.5. Selectivity, reproducibility, and stability

In order to study the selectivity, the DPV response of CBZ (50 µM) at Nd_2O_3/*f*-CNF/GCE was examined in the presence of various potentially interfering compounds, as shown in **Fig. 5C**. As all other interfering compounds (like pesticides, biological compounds, metal ions, and carbofuran, ascorbic acid, and caffeic acid) have not changed the oxidation peak current of CBZ, the calculated Relative standard deviation (RSD) values are below 3.8%, even when there are excessive amounts of other interfering compounds. According to the obtained results, the modified Nd_2O_3/*f*-CNF/GCE is highly selective for detecting CBZ. A relative error bar is shown in **Fig. 5D**. The CBZ oxidation peak current was not affected by the presence of interfering species; thus, it can be used for monitoring CBZ in real time.

A series of five Nd_2O_3/*f*-CNF/GCEs were prepared and tested for reproducibility in CBZ (50 μM) containing PBS using DPV. The fabricated eight electrodes show similar potential and peak current responses from the obtained DPV curves. The RSD of 3.42% was found for the reproducibility of eight sensors, which shows the excellent reproducibility of the fabricated sensor. The long-term stability of the Nd_2O_3/*f*-CNF/GCE was studied after 20 days of storage in a refrigerator (4°C). DPV performed periodic measurements of the oxidation current response to CBZ (50 μM) at the modified electrode. Despite the long-term stability of the electrode, the peak current value was still 97% of the original value after 22 days. The above results indicate that the modified Nd_2O_3/*f*-CNF/GCE sensor was both reproducible and stable toward the detection of CBZ.

3.6. Real sample analysis

We evaluated the practical feasibility of the proposed CBZ sensor to access practical applications. Analyses of real samples were performed using DPV under similar experimental conditions as those described in **Fig. 5A**. Various water (tap water, pond water, and portable water), soil, and vegetables (brinjals, cabbages, and carrots) samples were used for the real sample analysis. The vegetables were brought from a local market for real sample analysis. Samples of vegetables were cut into small pieces and ground with an electric blender before being analyzed. After collecting the extract, it was centrifuged for 15 minutes at 3000 RPM. The water samples were used directly for real sample analysis; only the pH was adjusted to 7.0 before the analysis. The soil sample was added to the PBS and filtered before analysis for real samples. The DPV test results found that the utilized water, vegetable, and soil samples were CBZ-free after diluting them with PBS. Then, DPV responses of real samples were studied when a known concentration of CBZ was added to the real samples. The standard addition method was used to calculate the recovery, and **Table 2** shows the concentration and recovery results of vegetables, water, and soil samples. The excellent recoveries of CBZ in different vegetables (97.4 – 99.2%), water (96.5 – 99.1%), and soil samples (95.8 – 97.4%) with appropriate relative standard deviation (RSD) were obtained using the fabricated electrode, indicating the excellent practicality of the fabricated sensor. These results confirmed the high accuracy in determining CBZ in the real samples.

Table 2 Determination of CBZ using the Nd_2O_3/*f*-CNF composite modified electrode in different water, vegetable, and soil samples.

Sample	Added (µM)	Found (µM)	Recovery	RSD (%)
Cabbage	5	4.79	98.0	2.1
	10	9.88	98.8	2.3
	20	18.62	97.4	1.3
	30	28.91	98.6	1.5
Brinjal	10	9.89	98.5	2.3
	20	18.99	98.7	3.4
	30	29.81	99.2	1.8
Carrot	10	8.64	97.6	2.3
	20	19.03	98.2	1.9
	30	28.45	98.7	2.6
Soil	10	9.62	96.2	3.4
	20	19.15	95.8	3.9
	30	29.22	97.4	3.7

Drinking water	10	9.91	99.1	1.6
	20	19.78	98.9	1.9
	30	29.65	98.8	1.5
Tap water	10	9.85	98.5	1.9
	20	19.56	97.8	2.4
	30	29.75	99.1	2.1
Pond water	10	9.65	96.5	3.6
	20	19.35	96.8	4.1
	30	29.45	98.2	4.0

4. Conclusions

In conclusion, a straightforward methodology has been used to synthesize the Nd_2O_3/*f*-CNF composite, and its modified electrode was used for the first time for the sensitive and low potential detection of CBZ. Microscopic examinations confirmed the presence of Nd_2O_3 nanoparticles on the surface of *f*-CNF. Also, the other physicochemical studies supported the successful formation of the Nd_2O_3/*f*-CNF composite. In electrochemical studies, it was found that the Nd_2O_3/*f*-CNF composite electrode had a greater surface area and more extraordinary electron transfer ability than Nd_2O_3 and *f*-CNF modified electrodes. The electroanalytical studies determined that the Nd_2O_3/*f*-CNF composite-modified electrode was highly sensitive toward CBZ detection, detecting CBZ at low levels of 4.3 nM with higher sensitivity (0.142 $\mu A \mu M^{-1}$) and providing a more comprehensive linear response range (up to 243 μM). The fabricated composite modified electrode showed excellent selectivity towards CBZ despite the influence of various interfering compounds, including similar insecticides. This excellent recovery of CBZ in water, vegetable, and soil samples confirmed the excellent practicality of the Nd_2O_3 and *f*-CNF-modified electrodes. The synthesized Nd_2O_3/*f*-CNF composite could be applied to environmental remediation in investigated water, vegetable, and soil samples.

Acknowledgments

The authors would like to thank the Khalifa University of Science and Technology and Yeungnam University for providing the necessary support for the study.

References

[1] R. Liu, B. Li, F. Li, V. Dubovyk, Y. Chang, D. Li, K. Ding, Q. Ran, G. Wang, H. Zhao, A novel electrochemical sensor based on β-cyclodextrin functionalized carbon nanosheets@carbon nanotubes for sensitive detection of bactericide carbendazim in apple juice, Food Chem. 384 (2022). https://doi.org/10.1016/j.foodchem.2022.132573.

[2] M.L. Yola, Carbendazim imprinted electrochemical sensor based on CdMoO4/g-C3N4 nanocomposite: Application to fruit juice samples, Chemosphere. 301 (2022) 134766. https://doi.org/10.1016/j.chemosphere.2022.134766.

[3] D. Ilager, S.J. Malode, N.P. Shetti, development of 2D graphene oxide sheets-based voltammetric sensor for electrochemical sensing of fungicide, carbendazim, Chemosphere. 303 (2022) 134919. https://doi.org/10.1016/j.chemosphere.2022.134919.

[4] L. Wei, X. Huang, J. Yang, Y. Wang, K. Huang, L. Xie, F. Yan, L. Luo, C. Jiang, J. Liang, T. Li, Y. Ya, A high performance electrochemical sensor for carbendazim based on porous carbon with intrinsic defects, J. Electroanal. Chem. 915 (2022). https://doi.org/10.1016/j.jelechem.2022.116370.

[5] Y. Li, X. Chen, H. Ren, X. Li, S. Chen, B.C. Ye, A novel electrochemical sensor based on molecularly imprinted polymer-modified C-ZIF67@Ni for highly sensitive and selective determination of carbendazim, Talanta. 237 (2022) 122909. https://doi.org/10.1016/j.talanta.2021.122909.

[6] D. Ilager, N.P. Shetti, Y. Foucaud, M. Badawi, T.M. Aminabhavi, Graphene/g-carbon nitride (GO/g-C3N4) nanohybrids as a sensor material for the detection of methyl parathion and carbendazim, Chemosphere. 292 (2022) 133450. https://doi.org/10.1016/j.chemosphere.2021.133450.

[7] A. Yamuna, T.W. Chen, S.M. Chen, Synthesis and characterizations of iron antimony oxide nanoparticles and its applications in electrochemical detection of carbendazim in apple juice and paddy water samples, Food Chem. 373 (2022) 131569. https://doi.org/10.1016/j.foodchem.2021.131569.

[8] J.F. de Macedo, A.A.C. Alves, M.V.S. Sant'Anna, F.G.C. Cunha, G. de A.R. Oliveira, L.M. Lião, E.M. Sussuchi, Electrochemical determination of carbendazim in grapes and their derivatives by an ionic liquid-modified carbon paste electrode, J. Appl. Electrochem. 52 (2022) 729–742. https://doi.org/10.1007/s10800-021-01665-8.

[9] H. Mahmoudi-Moghaddam, H. Akbari Javar, Z. Garkani-Nejad, Fabrication of platinum-doped NiCo2O4 nanograss modified electrode for determination of carbendazim, Food Chem. 383 (2022) 132398. https://doi.org/10.1016/j.foodchem.2022.132398.

[10] Q. Azizpour Moallem, H. Beitollahi, Electrochemical sensor for simultaneous detection of dopamine and uric acid based on a carbon paste electrode modified with nanostructured Cu-based metal-organic frameworks, Microchem. J. 177 (2022) 107261. https://doi.org/10.1016/j.microc.2022.107261.

[11] R. Elshafey, G.F. Abo-Sobehy, A.E. Radi, Imprinted polypyrrole recognition film @cobalt oxide/electrochemically reduced graphene oxide nanocomposite for carbendazim sensing, J. Appl. Electrochem. 52 (2022) 45–53. https://doi.org/10.1007/s10800-021-01613-6.

[12] L. Wang, S.A. Haruna, W. Ahmad, J. Wu, Q. Chen, Q. Ouyang, Tunable multiplexed fluorescence biosensing platform for simultaneous and selective detection of paraquat and carbendazim pesticides, Food Chem. 388 (2022) 132950. https://doi.org/10.1016/j.foodchem.2022.132950.

[13] N. Nataraj, T.W. Chen, M. Akilarasan, S.M. Chen, A.A. Al-Ghamdi, M.S. Elshikh, Se

substituted 2D-gC3N4 modified disposable screen-printed carbon electrode substrate: A bifunctional nano-catalyst for electrochemical and absorption study of hazardous fungicide, Chemosphere. 302 (2022) 134765. https://doi.org/10.1016/j.chemosphere.2022.134765.

[14] A. Özcan, F. Hamid, A.A. Özcan, Synthesizing of a nanocomposite based on the formation of silver nanoparticles on fumed silica to develop an electrochemical sensor for carbendazim detection, Talanta. 222 (2021). https://doi.org/10.1016/j.talanta.2020.121591.

[15] W. Zhong, F. Gao, J. Zou, S. Liu, M. Li, Y. Gao, Y. Yu, X. Wang, L. Lu, MXene@Ag-based ratiometric electrochemical sensing strategy for effective detection of carbendazim in vegetable samples, Food Chem. 360 (2021) 130006. https://doi.org/10.1016/j.foodchem.2021.130006.

[16] P. Sundaresan, C.C. Fu, S.H. Liu, R.S. Juang, Facile synthesis of chitosan-carbon nanofiber composite supported copper nanoparticles for electrochemical sensing of carbendazim, Colloids Surfaces A Physicochem. Eng. Asp. 625 (2021) 126934. https://doi.org/10.1016/j.colsurfa.2021.126934.

[17] C. Tian, S. Zhang, H. Wang, C. Chen, Z. Han, M. Chen, Y. Zhu, R. Cui, G. Zhang, Three-dimensional nanoporous copper and reduced graphene oxide composites as enhanced sensing platform for electrochemical detection of carbendazim, J. Electroanal. Chem. 847 (2019) 113243. https://doi.org/10.1016/j.jelechem.2019.113243.

[18] Y. Tan, S. Wei, X. Liu, B. Pan, S. Liu, J. Wu, M. Fu, Y. Jia, Y. He, Neodymium oxide (Nd2O3) coupled tubular g-C3N4, an efficient dual-function catalyst for photocatalytic hydrogen production and NO removal, Sci. Total Environ. 773 (2021) 145583. https://doi.org/10.1016/j.scitotenv.2021.145583.

[19] L. Liu, Y. Jia, X. Zhang, S. Chen, S. Wang, J. Zhu, L. Zheng, Z. Chen, L. Huang,

Identification of the function and regulatory network of circ_009773 in DNA damage induced by nanoparticles of neodymium oxide, Toxicol. Vitr. 78 (2022) 105271. https://doi.org/10.1016/j.tiv.2021.105271.

[20] K. Marquez-Mariño, J. Penagos-Llanos, O. García-Beltrán, E. Nagles, J.J. Hurtado, Development of a Novel Electrochemical Sensor Based on a Carbon Paste Electrode Decorated with Nd2O3 for the Simultaneous Detection of Tartrazine and Sunset Yellow, Electroanalysis. 30 (2018) 2760–2767. https://doi.org/10.1002/elan.201800550.

[21] Y. Zhou, Y. Li, P. Han, Y. Dang, M. Zhu, Q. Li, Y. Fu, A novel low-dimensional heteroatom doped Nd2O3 nanostructure for enhanced electrochemical sensing of carbendazim, New J. Chem. 43 (2019) 14009–14019. https://doi.org/10.1039/c9nj02778e.

[22] M. Arunpandian, K. Selvakumar, A. Raja, P. Rajasekaran, M. Thiruppathi, E.R. Nagarajan, S. Arunachalam, Fabrication of novel Nd 2 O 3 /ZnO-GO nanocomposite: An efficient photocatalyst for the degradation of organic pollutants, Colloids Surfaces A Physicochem. Eng. Asp. 567 (2019) 213–227. https://doi.org/10.1016/j.colsurfa.2019.01.058.

[23] V. Arancibia, J. Penagos-Llanos, E. Nagles, O. García-Beltrán, J.J. Hurtado, Development of a microcomposite with single-walled carbon nanotubes and Nd 2 O 3 for determination of paracetamol in pharmaceutical dosage by adsorptive voltammetry, J. Pharm. Anal. 9 (2019) 62–69. https://doi.org/10.1016/j.jpha.2018.11.005.

[24] A. Wahid, A.M. Asiri, M.M. Rahman, One-step facile synthesis of Nd2O3/ZnO nanostructures for an efficient selective 2,4-dinitrophenol sensor probe, Appl. Surf. Sci. 487 (2019) 1253–1261. https://doi.org/10.1016/j.apsusc.2019.05.107.

[25] H. Mohammad Shiri, A. Ehsani, Electrosynthesis of neodymium oxide nanorods and its nanocomposite with conjugated conductive polymer as a hybrid electrode material for

highly capacitive pseudocapacitors, J. Colloid Interface Sci. 495 (2017) 102–110. https://doi.org/10.1016/j.jcis.2017.01.097.

[26] R. Yuvakkumar, S.I. Hong, Nd2O3: novel synthesis and characterization, J. Sol-Gel Sci. Technol. 73 (2015) 511–517. https://doi.org/10.1007/s10971-015-3629-0.

[27] W. Yang, Y. Qi, Y. Ma, X. Li, X. Guo, J. Gao, M. Chen, Synthesis of Nd2O3 nanopowders by sol-gel auto-combustion and their catalytic esterification activity, Mater. Chem. Phys. 84 (2004) 52–57. https://doi.org/10.1016/j.matchemphys.2003.09.042.

[28] S. Đurđić, V. Stanković, F. Vlahović, M. Ognjanović, K. Kalcher, D. Manojlović, J. Mutić, D.M. Stanković, Carboxylated single-wall carbon nanotubes decorated with SiO2 coated-Nd2O3 nanoparticles as an electrochemical sensor for L-DOPA detection, Microchem. J. 168 (2021). https://doi.org/10.1016/j.microc.2021.106416.

[29] J. Tan, X. He, F. Yin, B. Chen, G. Li, X. Liang, H. Yin, Incorporating inactive Nd2O3 into Co/N-doped carbon as bifunctional oxygen electrocatalyst for rechargeable Zn-air battery, Catal. Today. 364 (2021) 67–79. https://doi.org/10.1016/j.cattod.2019.12.018.

[30] Z. Sabir, M. Akhtar, S. Zulfiqar, S. Zafar, P.O. Agboola, S. Haider, S.A. Ragab, M.F. Warsi, I. Shakir, L-Cysteine functionalized Nd2O3/rGO modified glassy carbon electrode: A new sensing strategy for the rapid, sensitive and simultaneous detection of toxic nitrophenol isomers, Synth. Met. 277 (2021) 116774. https://doi.org/10.1016/j.synthmet.2021.116774.

[31] A. Krishnapandi, S.M. Babulal, S.M. Chen, S. Palanisamy, S.C. Kim, M. Chiesa, Surface etched carbon nanofiber companied ytterbium oxide for pinch level detection of fungicides carbendazim, Journal of Environmental Chemical Engineering, 11 (2023) 109059. https://doi.org/10.1016/j.jece.2022.109059.

[32] A.S. Haidyrah, P. Sundaresan, K. Venkatesh, S.K. Ramaraj, B. Thirumalraj, Fabrication of functionalized carbon nanofibers/carbon black composite for electrochemical investigation of antibacterial drug nitrofurantoin, Colloids Surfaces A Physicochem. Eng. Asp. 627 (2021) 127112. https://doi.org/10.1016/j.colsurfa.2021.127112.

[33] M. Sakthivel, S. Ramaraj, S.M. Chen, B. Dinesh, H.V. Ramasamy, Y.S. Lee, Entrapment of bimetallic CoFeSe2 nanosphere on functionalized carbon nanofiber for selective and sensitive electrochemical detection of caffeic acid in wine samples, Anal. Chim. Acta. 1006 (2018) 22–32. https://doi.org/10.1016/j.aca.2017.12.044.

[34] S. Ramki, R. Sukanya, S.M. Chen, M. Sakthivel, Y.T. Ye, Electrochemical detection of toxic anti-scald agent diphenylamine using oxidized carbon nanofiber encapsulated titanium carbide electrocatalyst, J. Hazard. Mater. 368 (2019) 760–770. https://doi.org/10.1016/j.jhazmat.2019.01.110.

[35] D.N. Varun, J.G. Manjunatha, N. Hareesha, S. Sandeep, P. Mallu, C.S. Karthik, N.S. Prinith, N. Sreeharsha, S.M.B. Asdaq, Simple and sensitive electrochemical analysis of riboflavin at functionalized carbon nanofiber modified carbon nanotube sensor, Monatshefte Fur Chemie. 152 (2021) 1183–1191. https://doi.org/10.1007/s00706-021-02839-y.

[36] S. Ramki, R. Sukanya, S.M. Chen, M. Sakthivel, Hierarchical multi-layered molybdenum carbide encapsulated oxidized carbon nanofiber for selective electrochemical detection of antimicrobial agents: Inter-connected path in multi-layered structure for efficient electron transfer, Inorg. Chem. Front. 6 (2019) 1680–1693. https://doi.org/10.1039/c9qi00158a.

[37] S. Ramaraj, S. Mani, S.M. Chen, T. Kokulnathan, B.S. Lou, M.A. Ali, A.A. Hatamleh, F.M.A. Al-Hemaid, Synthesis and application of bismuth ferrite nanosheets supported

functionalized carbon nanofiber for enhanced electrochemical detection of toxic organic compound in water samples, J. Colloid Interface Sci. 514 (2018) 59–69. https://doi.org/10.1016/j.jcis.2017.12.016.

[38] R. Sukanya, M. Sakthivel, S.M. Chen, T.W. Chen, A new type of terbium diselenide nano octagon integrated oxidized carbon nanofiber: An efficient electrode material for electrochemical detection of morin in the food sample, Sensors Actuators, B Chem. 269 (2018) 354–367. https://doi.org/10.1016/j.snb.2018.05.013.

[39] P. Sundaresan, C.C. Fu, S.H. Liu, R.S. Juang, Facile synthesis of chitosan-carbon nanofiber composite supported copper nanoparticles for electrochemical sensing of carbendazim, Colloids Surfaces A Physicochem. Eng. Asp. 625 (2021) 126934. https://doi.org/10.1016/j.colsurfa.2021.126934.

[40] M. Sakthivel, S. Ramaraj, S.M. Chen, B. Dinesh, Synthesis of rose like structured LaCoO3 assisted functionalized carbon nanofiber nanocomposite for efficient electrochemical detection of anti-inflammatory drug 4-aminoantipyrine, Electrochim. Acta. 260 (2018) 571–581. https://doi.org/10.1016/j.electacta.2017.11.122.

[41] V. Muthulakshmi, C. Dhilip Kumar, M. Sundrarajan, Green synthesis of ionic liquid mediated neodymium oxide nanoparticles via Couroupita guianensis abul leaves extract with its biological applications, J. Biomater. Sci. Polym. Ed. 33 (2022) 1063–1082. https://doi.org/10.1080/09205063.2022.2039841.

[42] S. Yang, M. Yang, Q. Liu, X. Wang, H. Fa, Y. Wang, C. Hou, An Ultrasensitive Electrochemical Sensor Based on Multiwalled Carbon Nanotube@Reduced Graphene Oxide Nanoribbon Composite for Simultaneous Determination of Hydroquinone, Catechol and Resorcinol, J. Electrochem. Soc. 166 (2019) B547–B553.

https://doi.org/10.1149/2.0011908jes.

[43] García-Miranda Ferrari A, Foster CW, Kelly PJ, Brownson DAC, Banks CE. Determination of the Electrochemical Area of Screen-Printed Electrochemical Sensing Platforms. Biosensors. 8 (2018) 53. https://doi.org/10.3390/bios8020053.

[44] S. Periyasamy, J. Vinoth Kumar, S.M. Chen, Y. Annamalai, R. Karthik, N. Erumaipatty Rajagounder, Structural Insights on 2D Gadolinium Tungstate Nanoflake: A Promising Electrocatalyst for Sensor and Photocatalyst for the Degradation of Postharvest Fungicide (Carbendazim), ACS Appl. Mater. Interfaces. 11 (2019) 37172–37183. https://doi.org/10.1021/acsami.9b07336.

[45] Y. Dong, L. Yang, L. Zhang, Simultaneous electrochemical detection of benzimidazole fungicides carbendazim and thiabendazole using a novel nanohybrid material-modified electrode, J. Agric. Food Chem. 65 (2017) 727–736. https://doi.org/10.1021/acs.jafc.6b04675.

[46] C.A. Razzino, L.F. Sgobbi, T.C. Canevari, J. Cancino, S.A.S. Machado, Sensitive determination of carbendazim in orange juice by electrode modified with hybrid material, Food Chem. 170 (2015) 360–365. https://doi.org/10.1016/j.foodchem.2014.08.085.

[47] D. Wu, M. Wu, J. Yang, H. Zhang, K. Xie, C. Te Lin, A. Yu, J. Yu, L. Fu, Delaminated Ti3C2Tx (MXene) for electrochemical carbendazim sensing, Mater. Lett. 236 (2019) 412–415. https://doi.org/10.1016/j.matlet.2018.10.150.

[48] R. Cui, D. Xu, X. Xie, Y. Yi, Y. Quan, M. Zhou, J. Gong, Z. Han, G. Zhang, Phosphorus-doped helical carbon nanofibers as enhanced sensing platform for electrochemical detection of carbendazim, Food Chem. 221 (2017) 457–463. https://doi.org/10.1016/j.foodchem.2016.10.094.

[49] C. Tian, S. Zhang, H. Wang, C. Chen, Z. Han, M. Chen, Y. Zhu, R. Cui, G. Zhang, Three-dimensional nanoporous copper and reduced graphene oxide composites as enhanced sensing platform for electrochemical detection of carbendazim, J. Electroanal. Chem. 847 (2019) 113243. https://doi.org/10.1016/j.jelechem.2019.113243.

[50] L. Wei, X. Huang, J. Yang, Y. Wang, K. Huang, L. Xie, F. Yan, L. Luo, C. Jiang, J. Liang, T. Li, Y. Ya, A high performance electrochemical sensor for carbendazim based on porous carbon with intrinsic defects, J. Electroanal. Chem. 915 (2022). https://doi.org/10.1016/j.jelechem.2022.116370.

[51] Y. Zhou, R. Cui, Y. Dang, Y. Li, Y. Zou, Doping controlled oxygen vacancies of ZnWO4 as a novel and effective sensing platform for carbendazim and biomolecule, Sensors Actuators, B Chem. 296 (2019) 126680. https://doi.org/10.1016/j.snb.2019.126680.

[52] D. Ilager, H. Seo, S.S. Kalanur, N.P. Shetti, T.M. Aminabhavi, A novel sensor based on WO3·0.33H2O nanorods modified electrode for the detection and degradation of herbicide, carbendazim, J. Environ. Manage. 279 (2021) 111611. https://doi.org/10.1016/j.jenvman.2020.111611.

[53] A. Yamuna, T.W. Chen, S.M. Chen, T.Y. Jiang, Facile synthesis of single-crystalline Fe-doped copper vanadate nanoparticles for the voltammetric monitoring of lethal hazardous fungicide carbendazim, Microchim. Acta. 188 (2021). https://doi.org/10.1007/s00604-021-04941-8.

[54] R. Liu, Y. Chang, F. Li, V. Dubovyk, D. Li, Q. Ran, H. Zhao, Highly sensitive detection of carbendazim in juices based on mung bean-derived porous carbon@chitosan composite modified electrochemical sensor, Food Chem. 392 (2022) 133301. https://doi.org/10.1016/j.foodchem.2022.133301.

[55] A.M. Ashrafi, J. Dordević, V. Guzsvány, I. Švancara, T. Trtić-Petrović, M. Purenović, K. Vytřas, Trace determination of Carbendazim fungicide using adsorptive stripping voltammetry with a carbon paste electrode containing tricresyl phosphate, Int. J. Electrochem. Sci. 7 (2012) 9717–9731.

[57] W.F. Ribeiro, T.M.G. Selva, I.C. Lopes, E.C.S. Coelho, S.G. Lemos, F. Caxico De Abreu, V. Bernardo Do Nascimento, M.C. Ugulino De Araújo, Electroanalytical determination of carbendazim by square wave adsorptive stripping voltammetry with a multiwalled carbon nanotubes modified electrode, Anal. Methods. 3 (2011) 1202–1206. https://doi.org/10.1039/c0ay00723d.

Rational design of Nd_2O_3 decorated functionalized carbon nanofiber composite for selective electrochemical detection of carbendazim fungicides in vegetables, water, and soil samples

Selvakumar Palanisamy[a#*], Krishnapandi Alagumalai[b#], Matteo Chiesa[a, c*], Seong-Cheol Kim[b*].

[a]Laboratory for Energy and NanoScience (LENS), Khalifa University of Science and Technology, Masdar Campus, PO Box, 54224, Abu Dhabi, United Arab Emirates.

[b]School of Chemical Engineering, Yeungnam University, Gyeongsan 38541, Republic of Korea.

[c]Department of Physics and Technology, UiT The Artic University of Norway, 9010, Tromso, Norway.

[#]These authors contributed equally.

[*]Corresponding Authors

Selvakumar Palanisamy: prmselva@gmail.com

Matteo Chiesa: Email: matteo.chiesa@ku.ac.ae

Seong-Cheol Kim: Email: sckim07@ynu.ac.kr

Abstract

Abuse of carbendazim (CBZ) leaves excessive pesticide residues on agricultural products, which endangers human health because of the residues' high concentrations. Hence, a composite consisting of functionalized carbon nanofibers (*f*-CNF) with neodymium oxide (Nd_2O_3) was fabricated to monitor CBZ at trace levels. The Nd_2O_3/*f*-CNF composite-modified electrode displays higher electro-oxidation ability towards CBZ than Nd_2O_3 and *f*-CNF-modified electrodes. The combined unique properties of Nd_2O_3 and *f*-CNF result in a substantial specific surface area, superior structural stability, and excellent electrocatalytic activity of the composite yielding enhanced sensitivity to detecting CBZ with a detection limit of 4.3 nM. Also, the fabricated sensor electrode can detect CBZ in the linear concentration range of up to 243.0 μM with high selectivity, appropriate reproducibility, and stability. A demonstration of the sensing capability of CBZ in vegetables, water, and soil samples was reported paving the way for its use in practical applications.

Keywords: Fungicides detecting sensor; Carbendazim; Nd_2O_3; Functionalized carbon nanofibers composite; Electroanalysis

1. Introduction

Fungicides are frequently employed in modern agriculture to safeguard crops against fungi and boost yields [1,2]. Pesticide residues in the environment pose a severe risk to ecological safety, human health, food quality, and water supply [3]. Carbendazim (Methyl-2-benzimidazole carbamate, CBZ) is extensively used for crop protection and fast growth in the cultivation of various fruits and vegetables [4,5]. It can be utilized for pre-planting and post-harvesting in addition to seed storage before and after harvest [6,7]. However, prolonged or excessive exposure to CBZ can seriously damage soils, leading to contaminated groundwater and adverse effects on people and animals [8]. The benzimidazole ring attached to the structure of CBZ is responsible for the long-term stability and half-life of the compound (>3 years) [9]. Despite being banned in many countries, it is still used for plant cultivation because of its low cost and ability to accelerate growth [10]. Also, CBZ has been classified as a probable human carcinogen by the World Health Organization (WHO), and the multiplication of pesticide residues can cause severe adverse effects in humans and aquatic animals, including allergic reactions, dermatitis, eye irritation, hormonal abnormalities, infertility, teratogenicity, and mutagenicity [11,12]. This highlights the importance of concentrating on the quantitative development of efficient CBZ residue detection technologies. For identifying CBZ in various water sources, various cutting-edge analytical methods are available, including chemiluminescence, high-performance liquid chromatography, Raman scattering, UV-Vis spectrometry, and electrochemical detection [13,14,15]. Traditional chromatographic and spectroscopic techniques are sensitive, but they have certain drawbacks, such as the need for complex instrumentation, incapability for real-time observation, and length of time [16]. Electrochemical sensors have gained significant attention among other techniques because they are easy to use, high-accurate, inexpensive, quick, and use minimal chemicals [17].

Consequently, our approach to identifying CBZ in food samples was based on electrochemical methods.

The distinctive qualities of rare-earth metal oxides (La_2O_3, CeO_2, Pr_6O_{11}, and Nd_2O_3), such as electron richness in the d and f orbitals, catalytic effectiveness, optical, magnetic, and thermal stability, are what make them so popular for a variety of applications [18,19]. Among the lanthanide family, neodymium oxide (Nd_2O_3) is a more reactive oxide found naturally over most of the earth's crust. Also, Nd_2O_3 has been widely used in solar cells, lithium-ion batteries, supercapacitors, and sensors due to its improved catalytic and electric properties [23,24]. To date, various synthesis methods have been used to synthesize Nd_2O_3, including hydrothermal synthesis, sol-gel auto combustion, template synthesis, polyol synthesis, microemulsion synthesis, inductively coupled radiofrequency thermal plasma, and micro-aided synthesis [25-27]. Nevertheless, the improvements on single metal oxides still suffer from poor applicability, low conductivity, and unsatisfactory cyclic stability during the chemical reaction [28]. Therefore, developing a carbon matrix that can be modified efficiently to enhance the electrocatalyst for environmental hazards sensors is imperative [29,30]. Our previous study revealed that lanthanide oxides with functionalized carbon nanofibers (*f*-CNF) could selectively detect CBZ with improved sensitivity [31]. The surface properties of *f*-CNF are similar to those of other carbon nanomaterials (graphene oxide and functionalized carbon nanotubes), which makes it suitable for electrochemical sensor applications [32-34]. Furthermore, *f*-CNF has many free hydroxyl groups on its cylindrical surface, which makes it an ideal material to disperse in an aqueous solution. [35]. As a result of its unique surface properties and cylindrical nanostructure nature, *f*-CNF would significantly boost the electron conductivity and electrochemical performance of lanthanide oxides [31]. According to a literature survey, *f*-CNF-based composite materials have been used for the electrochemical determination of various analytes, including CBZ [31-40]. As far as we know, there is no report on the detection of CBZ utilizing Nd_2O_3 with *f*-CNF nanocomposite. The Nd_2O_3/*f*-CNF modified electrode was employed for the sensitive and lower potential detection of CBZ by cyclic voltammetry (CV) and differential pulse voltammetry (DPV) for electrochemical sensor applications. The fabricated sensor displayed a more comprehensive linear range, a lower detection threshold, and good sensitivity. Additionally, it demonstrated respectable applicability for examining CBZ in real samples, such as beet, carrot, and cabbage.

2. Experimental section

2.1. Materials and reagents

Neodymium (III) chloride (99.9% trace metals basis), ethylene glycol, Urea, malathion, parathion, thiamethoxam, carbofuran, ascorbic acid, caffeic acid, and carbendazim were purchased from Sigma-Aldrich and used without any further purification. Carbon nanofibers (98% amorphous carbon with iron impurities below 14000 ppm, diameter =100 mm, length = 20-200 µm, and surface area 39 m^2/g) were purchased from Sigma-Aldrich. Monosodium phosphate (≥99%) and disodium phosphate (≥98.5%) were used to make different concentrations supporting electrolyte solution during electrochemical analysis, and HCl and NaOH were used to adjust the pH value. All other chemicals used in this study were purchased from Sigma-Aldrich and used as received.

2.2. Synthesis and fabrication of Nd_2O_3/*f*-CNF modified electrode

The Nd_2O_3 was synthesized via a cost-effective familiar coprecipitation method. In general, 0.1 M of $Nd(NO_3)_3.6H_2O$ was dissolved in 40 mL of deionized (DI) water and allowed to continue stirring at room temperature. About 10.0 mL of ethylene glycol was added slowly into the above mixture and stirred for 90 minutes at 4000 RPM. A white and homogeneous precipitate was obtained at the end of the reaction. The reaction mixture in the beaker was kept under an ultrasonication bath for 1 h for homogeneous formation. The settled residue was washed with DI water and ethanol 3 times before centrifuging at 4000 rpm to remove external impurities. Afterward, the obtained precipitates were dehydrated at 55 ºC for 24 h. The synthesized product (Nd$_2$O$_3$) was calcined at 500 ºC for 6 h and used for further characterization. The *f*-CNF was synthesized using an acid functionalization method reported early [31].

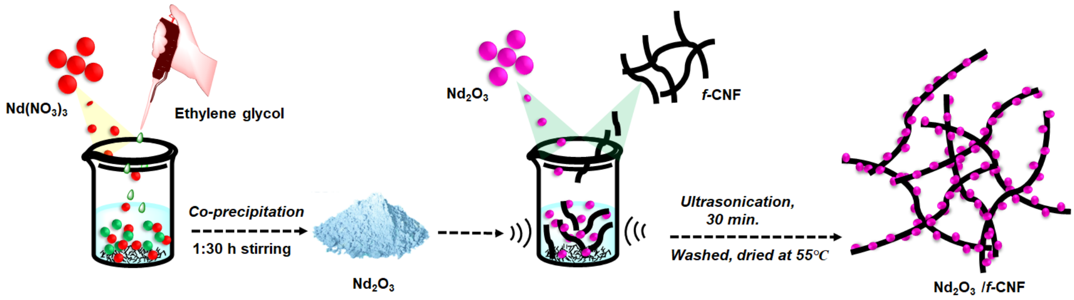

Scheme 1. A schematic representation of the overall synthesis process of Nd$_2$O$_3$/*f*-CNF composite.

As preparation for the electrocatalyst, 8 mg of Nd$_2$O$_3$ and 4 mg *f*-CNF were added to the vial containing DI water. The mixture was kept under the ultrasonic bath and sonicated until a homogenous suspension was obtained. Afterward, the suspension was centrifuged at 4000 rpm for 15 minutes and washed numerous times with DI water and ethanol to remove impurities. The obtained Nd$_2$O$_3$/f-CNF was dried at 80 °C for 8 h. Oxidized carboxylic functional groups in *f*-CNF allow the Nd$_2$O$_3$ nanoparticles to adhere well to the outer interlayers of the structure during ultrasonication. A schematic representation of the overall synthesis process of the Nd$_2$O$_3$/*f*-CNF composite is shown in **Scheme 1**. We prepared the Nd$_2$O$_3$/*f*-CNF composite dispersion by ultrasonically dispersing 3 mg of the composite in 1 mL of DI water for 15 minutes at room temperature. After that, the Nd$_2$O$_3$/*f*-CNF composite dispersion was drop cast (6 µL) over the glassy carbon electrode (GCE) surface, and the suspension was allowed to dry at ambient temperature. The fabricated Nd$_2$O$_3$/*f*-CNF composite electrode was further used for the electrochemical/catalytic studies, and the same electrode preparation procedure was used for all experiments.

2.3. Apparatus and measurements

Powder X-ray diffraction (XRD) patterns of synthesized Nd_2O_3, *f*-CNF, and Nd_2O_3/*f*-CNF composite were studied using a PAN analytical X'Pert PRO diffractometer with Cu Kα radiation (λ = 1.5418 Å). Each sample's crystal structure was investigated in the 10-90° 2θ with a 0.02° step size. IR spectrum of the synthesized samples was recorded using a KBr disc on a JASCO Fourier transform infrared (FT-IR) 460 Plus spectrophotometer. A Raman spectrometer with a charge-coupled detector (Dong Woo 500i, Korea) was used to investigate particle size, morphology, and vibration modes. X-ray photoelectron spectroscopy (XPS) analyzed the prepared samples' elemental composition and oxidation state (XPS, Thermo Scientific Multi-Lab 2000). A High-Resolution Transmission Electron Microscope (HR-TEM): JEOL 2100F was used for scanning images, selected area electron diffraction (SEAD), and elemental mapping. The pH of the sample was measured with a Horiba-L aqua pH meter calibrated with a standard buffer of the relevant pH.

The electrochemical experiments were carried out using a conventional three-electrode system equipped with a modified GCE as a working electrode, a platinum wire as an auxiliary electrode, and Ag/AgCl (sat.KCl) as a reference electrode. Alumina-silica powder was used to clean all electrodes before beginning electrochemical experiments. A CHI 750A electrochemical workstation (CH Instruments, USA) was used for the electrochemical studies, including CV and DPV experiments.

3. Results and Discussion

3.1. Characterization

The HR-TEM was used to analyze the surface morphology of as-synthesized *f*-CNF, Nd_2O_3, and Nd_2O_3/*f*-CNF composite. In **Fig.1A**, the TEM image of the *f*-CNF clearly shows stacked-cup carbon nanofibers, which are visible in the magnified image. It was calculated that the average diameter and width of the *f*-CNF are 226 nm and 142 nm, respectively. In **Fig.1B** and **C**, the sphere-like structure of the Nd_2O_3 nanoparticles can be seen with a uniform size of around 80-100 nm with a diameter of 160-200 nm. A TEM image of the Nd_2O_3/*f*-CNF composite (D-E) revealed successful embattlement of Nd_2O_3 nanoparticles on the surface of *f*-CNF. Also, the Nd_2O_3 nanoparticles were evenly attached with slight aggregation (**Fig.1F**).

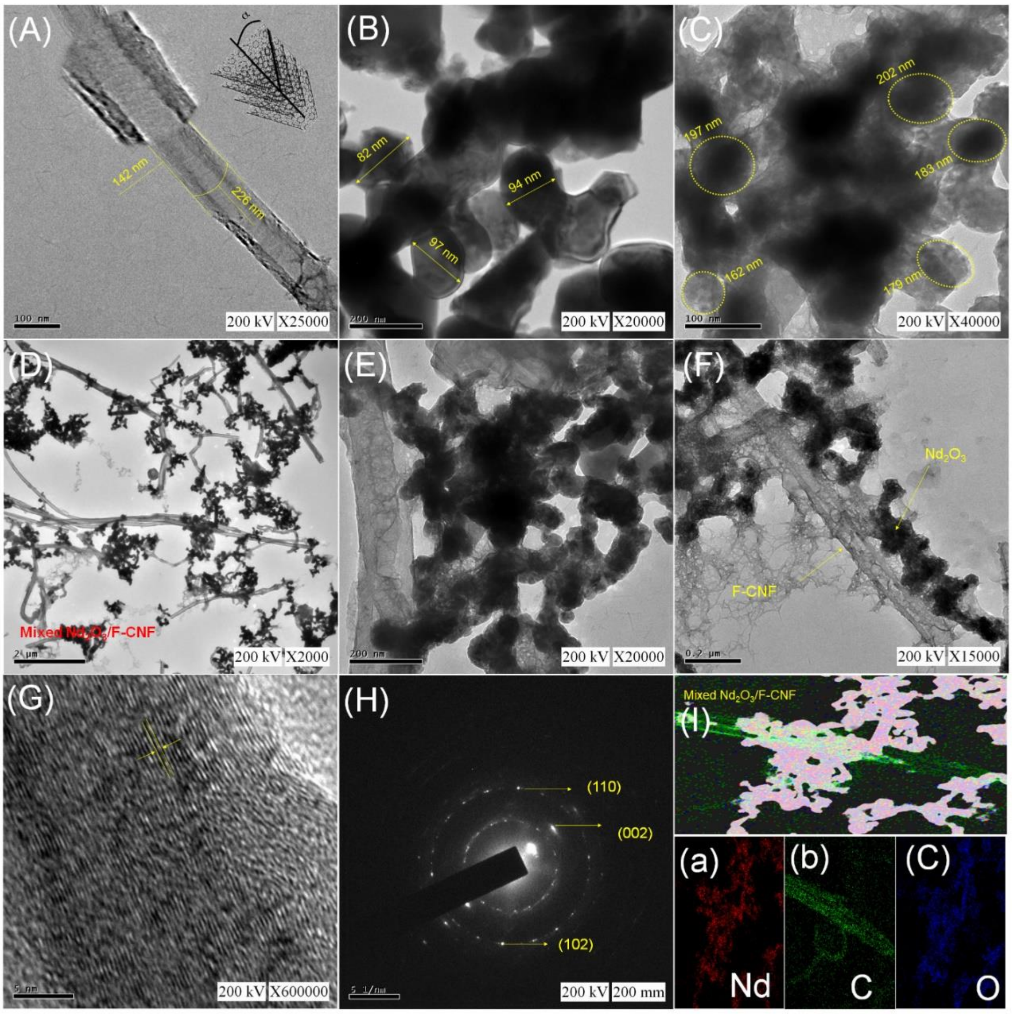

Figure 1. HR-TEM images of (A) *f*-CNF, (B, C) Nd_2O_3, and Nd_2O_3/*f*-CNF composite in different magnifications (D-F), Lattice fringe for Nd_2O_3 (G). SEAD pattern of Nd_2O_3, and elemental mapping of Nd, C, and O for Nd_2O_3/*f*-CNF composite.

The (111) plane of the *f*-CNF was attributed to the lattice fringe distance of 0.21 nm, and a well-resolved Nd_2O_3 crystal ring pattern was observed in **Fig. 1G**, whose ring spots matched XRD plane values including (110), (002), and (102) (**Fig. 1H**). The results confirmed that the high crystal nature of Nd_2O_3 was unaffected by *f*-CNF in the Nd_2O_3/*f*-CNF composite. In **Fig. 1I**, we see that the Nd (a), O (b), and C (c) are evenly distributed throughout the Nd_2O_3/f-CNF composite, indicating that the fabrication was successful and uninterrupted.

Fig. 2A of the Raman spectra of Nd_2O_3 show the lower and higher number bands at 90.1, 121, 133.5, 195.3, 338.4, 431.6, 546.5, and 1009.2, 1077.3, 1356.7, 1611.2, 1927 cm^{-1}, which relate to Fg and Ag + Eg modes, respectively [41]. The Raman spectra of the *f*-CNF show that the D and G bands at 1348 and 1589 cm^{-1} result from disordered and ordered graphitic carbon on CNF [26]. In contrast, the decrease in G-band intensity indicates a low level of impurities and high crystallinity of CNF. In addition, the graphitic carbon (G band) and carbon (D band) of the *f*-CNF are arranged orderly, which means that no defects are observed in the *f*-CNF. The contrast between the *f*-CNF and Nd_2O_3, the Nd_2O_3/*f*-CNF composite peak intensity indicates disorder in the sp^2 carbon lattice and compressive strains induced by the bonds between *f*-CNF and oxygen adsorption on surfaces of transition metal oxides. FTIR spectroscopy was used to identify the functional groups in Nd_2O_3 nanoparticles, *f*-CNF, and Nd_2O_3/*f*-CNF nanocomposite. As shown in **Fig. 2B**, the broad peak at 3490 - 3600 cm^{-1} corresponds to the -OH stretching vibration, while the broad blend peak at 1639 cm^{-1} is attributed to the CO stretching vibration. The two significant peaks at 566 cm^{-1} and 725 cm^{-1} are related to the Nd-O stretching vibration (metal-oxygen bond), showing the formation of Nd_2O_3 nanoparticles [25]. Three other series peaks between 1030 and 1232 cm^{-1} are associated with the stretching vibration of the carbon and hydroxyl group (C-OH) bond. The broader peaks 1048 and 1526 cm^{-1} are according to the asymmetric and symmetric vibrations of the O-C-O bond. FTIR spectrum of *f*-CNF revealed the following peaks at 1225.7, 1538.8, 1646, 1701, and 3462 cm^{-1}, which correspond to the acid-treated functional groups C-O, C=C, C-O-C, C=O, and -OH [42]. This was similar to the peak observed in the Nd_2O_3/*f*-CNF composite, which confirmed the presence of *f*-CNF and Nd_2O_3. Also, the Raman spectra of *f*-CNF exhibited two distinct peaks at 1362 cm^{-1} and 1606 cm^{-1}, which are attributed to the D band and G band, indicating the successful formation of *f*-CNF. An XRD analysis was performed to determine the phase purity and crystal structure of the as-synthesized Nd_2O_3, *f*-CNF, and Nd_2O_3/*f*-CNF composites.

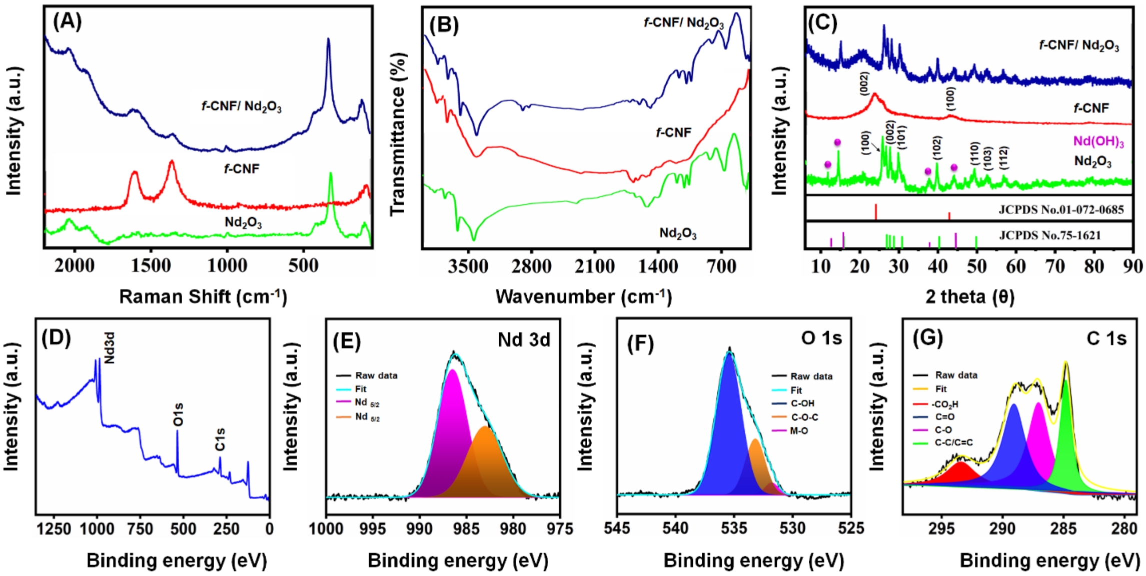

Figure 2. A) Raman, (B) FTIR and C) XRD spectra of *f*-CNF, Nd_2O_3, and Nd_2O_3/*f*-CNF composite, D) Survey spectra of Nd_2O_3/*f*-CNF composite and (E-G) individual XPS spectra of Nd 3d, C 1s, and O 1s.

Fig. 2C displays the XRD pattern of Nd_2O_3. As visible in **Fig. 2C**, the diffraction peaks at 2θ of 27.0°, 28.8°, 30.8°, 40.4°, 49.6°, 52.9°, and 57.1° are associated with hexagonal phases (100), (002), (101), (102), (110), (103), and (112) and are well-matched with the previously reported literature [JCPDS:00-43-102] [28]. Using Debye-Scherrer's equation (1), we calculated the average crystalline size of Nd_2O_3.

$$D_{XRD}= {}^{K\lambda}/_{\beta_{hkl}COS\theta} \qquad (1)$$

Where λ is the wavelength of X-ray (0.15406 Å), D represents the size of crystallites (nm), q is the diffraction angle, k is a constant value, and β is full with half maximum (FWHM) of the diffraction peak. The calculated average crystalline size (D) of the Nd_2O_3 was 63.1 nm. The results show that the synthesized Nd_2O_3 consists only of Nd, O, and no other impurities. Several other peaks were also observed at 13.2°, 15.7°, 38.3°, and 42.6°, which correspond to the hexagonal structure of $Nd(OH)_3$. According to the XRD pattern of the *f*-CNF, the peaks at 24.4° and 42.2° were well indexed with (002) and (100), respectively, indicating the presence of a carbon source [35]. The presence of *f*-CNF partially influenced Nd_2O_3, and accordingly, some combinations disappeared because of *f*-CNF. Additionally, XPS spectra of Nd_2O_3/f-CNF nanocomposite revealed its chemical composition and oxidation state. As shown in **Fig. 2D**, the Nd_2O_3/*f*-CNF composite spectra are located at 985.5, 355.6, and 286.9eV, indicating the presence of Nd 3d, O1s, and C 1s. **Fig. 2D** shows the Nd 3d XPS spectrum of Nd_2O_3 at 986.3 eV, which is further deconvoluted into two Nd^{3+} peaks at 982.3 eV and 986.1 eV corresponding to Nd $3d_{5/2}$. In **Fig. 2F**, the O1s peaks correspond to the aromatic C-OH, C-O-C, and M-O bonds (metal-oxygen bonds). Also, the C 1s spectrum of **Fig. 2G** show four different oxygen peaks at binding energies of 294.1, 289.4, 286.8, and 285.1; these correspond to functional groups such as $-CO_2H$, C=O, C-O, and Sp^3/Sp^2 orbital bonds in the surface of the Nd_2O_3/*f*-CNF composite [36]. The above results confirmed the successful formation of Nd_2O_3/*f*-CNF nanocomposite.

3.2. Electrochemical and catalytic properties of the modified electrode

The electron transfer and electroactive surface area of different electrodes were determined using CV. A mixed solution of 0.5 M $Fe(CN)_6^{3-/4-}$ and 0.1 M KCl was used to test the electrochemical performance of the modified and unmodified electrodes. According to **Fig. 3A**, the bare GCE displays a weak redox peak response due to a low electron transfer rate. After GCE was modified with Nd_2O_3, *f*-CNF, and Nd_2O_3/*f*-CNF, the redox peak current of GCE gradually increased. From these experiments, Nd_2O_3/*f*-CNF/GCE show a higher redox peak current than other electrodes, possibly because the Nd_2O_3 interacts with the surface-etched f-CNF with a strong π-π bond, which can result in improved electrocatalytic activity and electron transfer kinetics in Nd_2O_3/*f*-CNF/GCE.

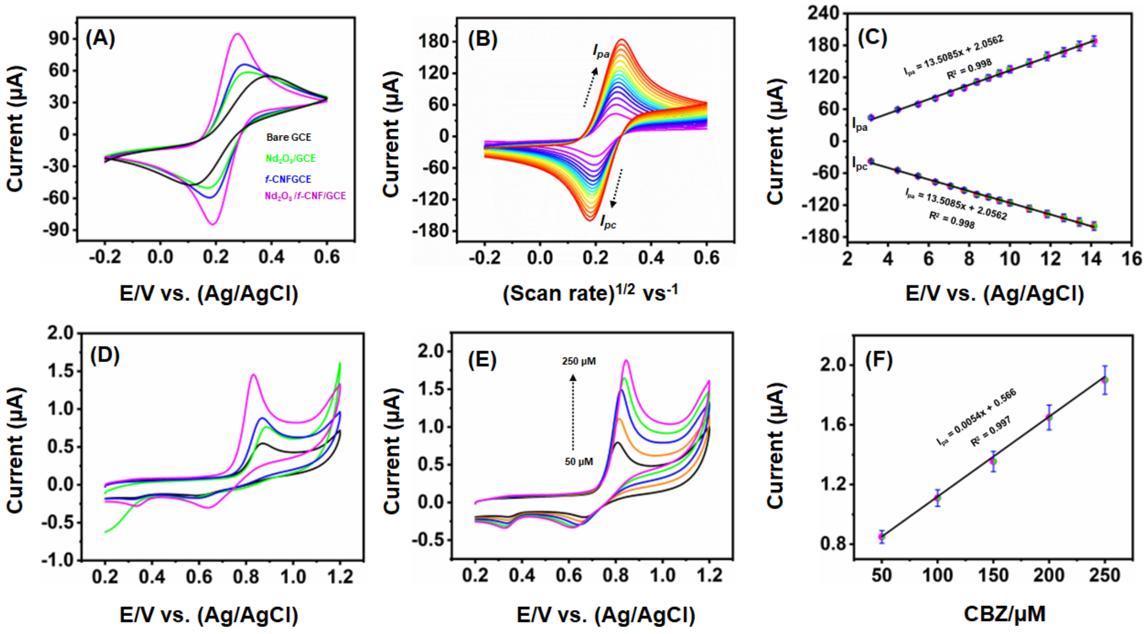

Figure 3. A) CV response of bare GCE, Nd_2O_3/GCE, *f*-CNF/GCE, and Nd_2O_3/*f*-CNF/GCE in 0.5 M of $[Fe(CN)_6]^{3-/4-}$ comprises 0.1 M of KCl at a scan rate of 50 mV s^{-1}. B) At the same conditions, the CV response of Nd_2O_3/*f*-CNF/GCE at different scan rates from 10 to 200 mV s^{-1}. C) The linear relationship between the square root of scan rate (mV s^{-1}) *vs.* anodic and cathodic peak current (I_{pa} and I_{pc}) response. D) CV curves of different electrodes at scan rate 50 mVs^{-1} in the presence of 100 μM CBZ in PH 7.0. The color description for the different electrodes is the same as in (A). E) CV response for adding different quantities of CBZ (50-250 μM) on Nd_2O_3/*f*-CNF/GCE in pH 7.0 at a scan rate of 50 mV s^{-1}. F) The linear relationship between the [CBZ] *vs.* I_{pa}.

We also measured the electroactive surface area of the unmodified and modified electrodes in a mixed solution of 0.5 M $Fe(CN)_6^{3-/4-}$ and 0.1 M KCl solution at various scan rates from 10 to 200 mV s^{-1} (**Fig. 3B**). The results confirmed that the square root of scan rates had linear dependence with the anodic and cathodic peak current response of the Ferro/Ferri redox couple (**Fig. 3C**). Electroactive surface area of various modified GCEs were calculated using Randles–Ševćik equation for reversible electrochemical processes [**43**]. Using the Rendles-Sevick equation (2), the active surface areas of the Nd_2O_3/GCE, *f*-CNF/GCE, and Nd_2O_3/*f*-CNF/GCE were calculated to be 0.079, 0.088, and 0.094 cm^{-2}, respectively.

$$I^{rev} = 0.446\, n\, FA_{real}\, C \sqrt{\frac{nFDv}{RT}} \ldots\ldots\ldots\ldots\ldots\ldots\ldots\ldots\ldots\ldots\ldots\ldots\ldots \text{(2)}$$

Where I^{rev} is the redox peak current (μA), *A* is the electroactive surface area (cm^2), A is the surface area of the electrode, C is the concentration, *D* is the diffusion coefficient (7.6 x 10^{-6}), and *n* is the number of electrons (n=1), and *v* is scan rate (Vs^{-1}). Also, the % of real and geometrical surface area of bare GCE was calculated using %real = (A_{real}/A_{geo}) × 100). The % of real was 86.1% when compared to the active surface area of 0.068 cm^2. The above results make clear that the Nd_2O_3/*f*-

CNF/GCE has a higher electroactive surface area among the other electrodes and can be used for the enhanced electrochemical detection of CBZ.

The electrochemical response of different electrodes was examined by CV with 100 µM CBZ in 0.1 M PBS (pH 7.0) at a scanning rate of 50 mVs^{-1} with the potential scanning from 0.3 to 1.3 V. The color description for the different electrodes is the same as in **Fig. 3A**. As shown in **Fig. 3D**, the bare GCE exhibits a low oxidation peak current of 0.61 µA response with the higher oxidation potential (E_{pa}) due to low electron transfer kinetics and poor catalytic performance. The peak current and peak potential of modified electrodes gradually increased, as shown in **Fig. 3D**, Nd_2O_3/GCE (I_{pa} = 0.75 µA, E_{pa} = 0.839 V)>*f*-CNF/GCE (I_{pa} = 0.85 µA, E_{pa} = 0.816 V)> Nd_2O_3/*f*-CNF/GCE (I_{pa} = 1.5 µA, E_{pa} = 0.8 V). Compared with other electrodes, the Nd_2O_3/*f*-CNF/GCE exhibited a higher oxidation peak current response and a lower oxidation peak potential, indicating that the Nd_2O_3/*f*-CNF composite modified electrode can be used for sensitive and lower potential detection of CBZ. The combined unique properties of *f*-CNF and Nd_2O_3 through π-π interactions had a synergistic effect on enhancing the electrocatalytic activity against CBZ oxidation. The anodic peak in carbendazim comes from the oxidation of nitrogen atoms in the pyridine ring of benzimidazole. The possible oxidation mechanism of CBZ on the Nd_2O_3/*f*-CNF composite-modified electrode is elucidated in **Scheme 2** [31].

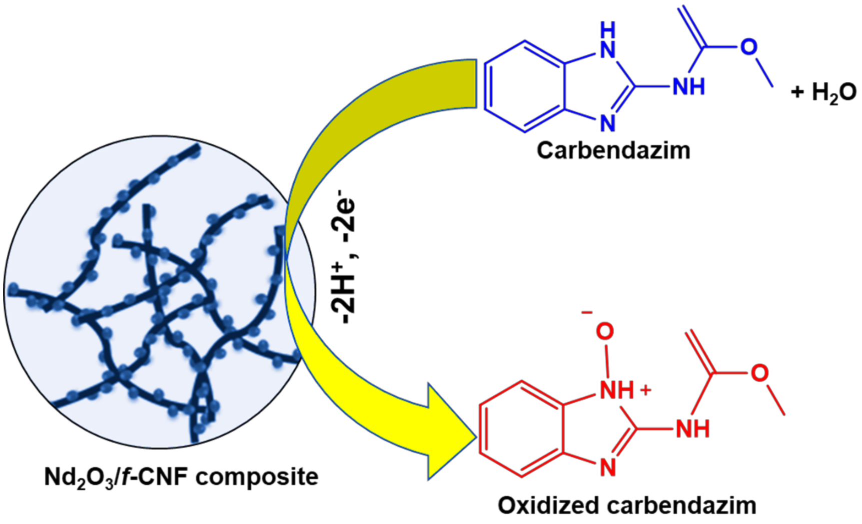

Scheme 2 Possible electrochemical oxidation mechanism of CBZ on Nd_2O_3/*f*-CNF composite modified electrode.

A quantitative assessment of CBZ was performed by CV at various concentrations (50-250 µM) in 0.1 M PBS at 50 mVs^{-1} (**Fig. 3E**). As concentrations of CBZ increased linearly, their peak currents also increased, and their potential shifted slightly from its original potential. As shown in **Fig. 3F**, the linear regression equation for the oxidation peak current is $I_{pa} = 0.0054[CPZ] + 0.566$ ($R^2 = 0.991$). The results indicate the excellent kinetics and higher electrocatalytic activity of Nd_2O_3/*f*-CNF/GCE towards CBZ.

3.3. Influence of scan rate and pH

We examined the impact of various scan rates on CBZ detection at Nd_2O_3/*f*-CNF/GCE in 0.1 M PBS (pH 7.0) containing CBZ (100 µM), as shown in **Fig. 4A**. As the scan rate increased, the oxidation peak current of CBZ also increased, and the peak current in the potential range was proportional to the scan rate obtained. This was described using the equation $I_{pa} = 0.0085v + 0.3169$ (R2=0.994) as the relationship plot between scan rates (mVs^{-1}) vs. I_{pa}. Further, the linear relationship between reduction peak current vs. scan rate (mVs^{-1}) is $I_{pc} = 0.1647v + 0.3889$ ($R^2 = 0.96$). The result implies that the electrochemical reaction of CBZ on the Nd_2O_3/*f*-CNF/GCE is the surface adsorption-controlled electrochemical reaction [**31**]. We examined the effect of pH for CBZ sensing (100 µM) at Nd_2O_3/*f*-CNF/GCE by using different pH (3.0 - 11.0) at a scan rate of 50 mV s^{-1} (**Fig. 4C**). By varying the pH of an electrolyte containing CBZ from low to high, the peak current and potential have moved towards the negative range, suggesting that protons are involved in the electrode reaction. In this study, pH 7.0 was determined to be the optimal pH value based on the maximum oxidation current observed. It was found that E_{pa} (V) = -0.0715 pH + 1.3115 ($R^2 = 0.998$) for different pH versus E_{pa} (V), which indicates the linear dependence of E_{pa} in a broader pH range.

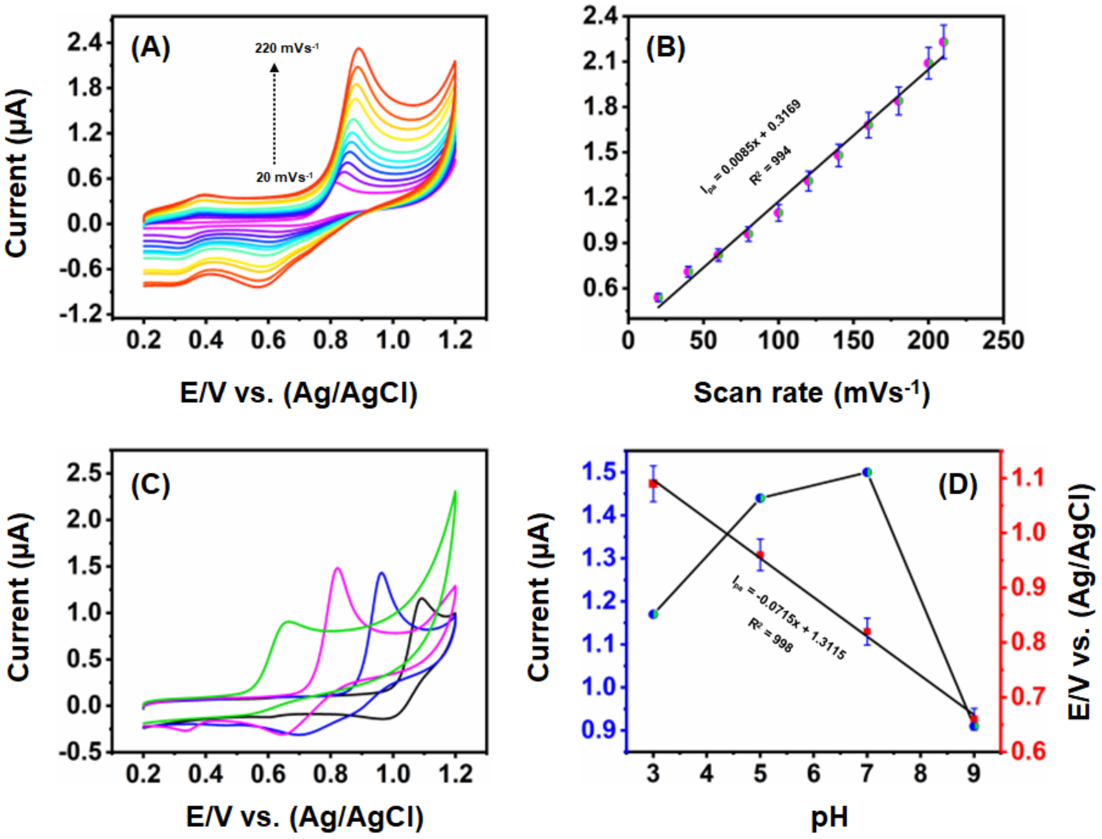

Fig. 4. A) CV response for CBZ (200 μM) at Nd_2O_3/*f*-CNF/GCE with different scan rates (20–220 mVs^{-1}). B) The linear relationship between the different scan rates *vs.* I_{pa}. C) CV response at Nd_2O_3/*f*-CNF/GCE with 100 μM CBZ containing different pH (pH 3.0–7.0) at scan rate 50 mVs^{-1}. D) The linear relationship between the pH *vs.* I_{pa} and E_{pa}.

3.4. Determination of CBZ at Nd_2O_3/*f*-CNF/GCE

In contrast to other electrochemical approaches, DPV has a higher detection sensitivity and a lower detection limit, making it an ideal technique for determining CBZ. **Fig. 5A** shows the DPV response current of CBZ at the Nd_2O_3/*f*-CNF/GCE for different concentration addition of CBZ, ranging from 0.1 to 243 μM. Under optimized conditions, the response current of CBZ shows a significantly enhanced trend upon increasing the CBZ concentration from 0.1 to 243 μM.

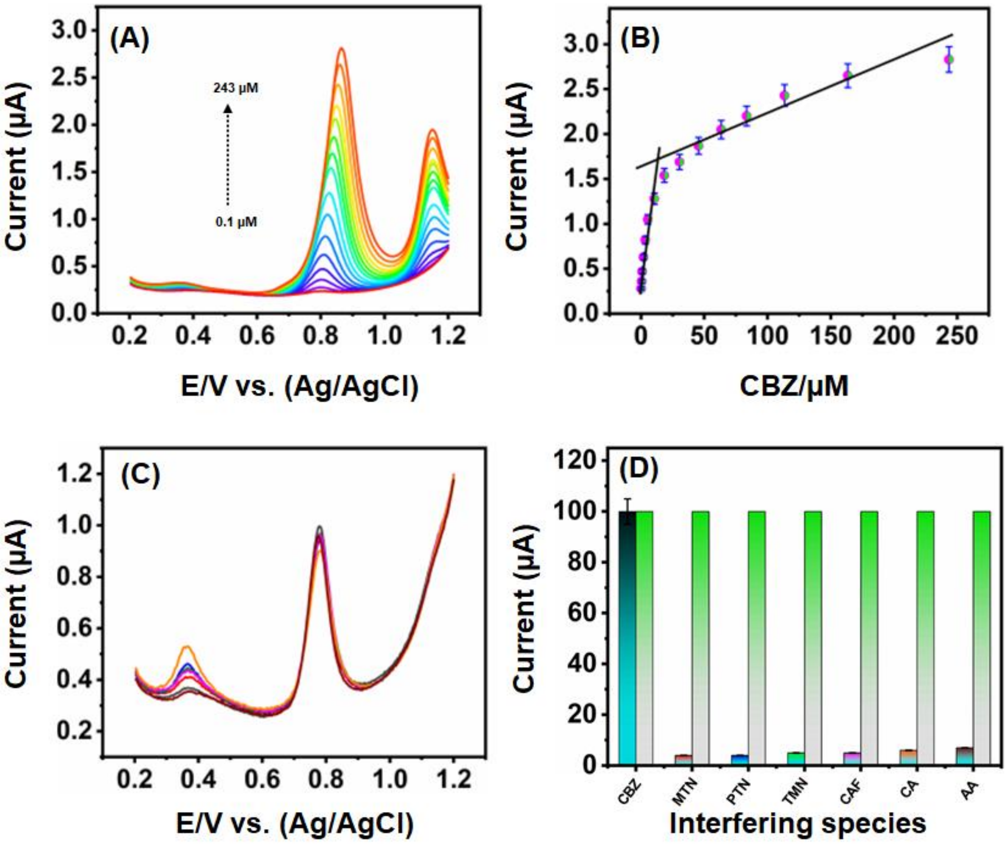

Figure 5. A) DPV curves of the Nd_2O_3/*f*-CNF/GCE for the successive addition of CBZ from 0.1 to 243 µM in pH 7.0. B) The linear relationship between the [CBZ] *vs.* I_{pa}. C) Selectivity of the sensor in the presence of co-inferring species and its corresponding error bar diagram (D).

Based on the DPV results, two linear curves are plotted at low and high CBZ concentrations. According to the first linear equation, I_{pa} (A) = 0.142 *C*[CBZ] +0.3152 ($R^2 = 0.984$) in the concentration range of 0.1-5.4 µM for CBZ. In the CBZ concentration range of 10.4-243 µM, the second equation is expressed as I_{pa} (A) = 0.0064 *C*[CBZ] + 1.5114 ($R^2 = 0.895$). Due to the empty free active sites on the electrode surface, CBZ is rapidly adsorbed on the electrode surface when injected consecutively. With high concentration, the CBZ curves shifted toward a more positive region with a low oxidation current. Also, the oxidation of CBZ at modified Nd_2O_3/*f*-

CNF composite surfaces is slightly slower because there are fewer unoccupied active sides. Since the occupied sites revealed low electroactive area and sensitivity, the first linear equation was used to calculate the sensor's low detection limit (LOD) and sensitivity. The calculated LOD is 4.3 nM (3Sd/N, where Sd is the standard deviation of blank and N is the slope of the calibration plot) and the analytical sensitivity are 0.142 µA μM^{-1} (slope of the calibration plot). The LOD of the sensor (100 nM) is lower than the WHO-recommended value for water samples. The fabricated sensor's analytical performance was compared with previously reported CBZ sensors to confirm the developed sensor's novelty. Comparative results between the Nd_2O_3/*f*-CNF/GCE sensor and those previously reported in the literature are shown in **Table 1**. Notably, the Nd_2O_3/*f*-CNF/GCE has lower LOD (4.3 nM) than previously used CBZ sensors based on the composites of single and multiwalled carbon nanotubes ($ZnFe_2O_4$/SWCNT and SiO_2/MWCNT), phosphorus-doped helical carbon nanofibers (HCNFs), reduced graphene oxide composites (NP-Cu/RGO and QD-rGO). Also, the sensitivity and linear response of the fabricated sensor is enhanced and comparable to the previously reported CBZ sensors listed in **Table 1**. Therefore, the Nd_2O_3/*f*-CNF composite-modified electrode is a promising alternative electrode material for sensitive and low levels detection of CBZ in environmental samples.

Table 1 Analytical comparison of Nd_2O_3/*f*-CNF composite modified electrode with previously reported modified electrodes for the determination of CBZ.

Electrode	**Linear range (µM)**	**Limit of detection (nM)**	**Sensitivity (µA/µM)**	**Refs.**
La-Nd_2O_3/CPE	0.08-50	27	NR	[21]
Yb_2O_3/f-CNF/GCE	0.05 to 3035	6	0.049	[31]
$ZnFe_2O_4$/SWCNT/GCE	0.5-100	90	NR	[45]
SiO_2/MWCNT/GCE	0.2-4.0	56	0.485	[46]
Ti_3C_2TxMXene/GCE	0.05-100	10.3	NR	[47]
P-HCNFs/GCE	1-35	38	0.92	[48]
NP-Cu/RGO/GCE	0.5-30	90	0.085	[49]
D-PC/GCE	0.01-1.00	6	NR	[50]
Ce-dope $ZnWO_4$/GCE	0.01-5.5	3	0.0289	[51]
$WO_{3.0}$.33H_2/GCE	0.1-250	22	NR	[52]
Fe-CuV/GCE	0.01-83.1	5	0.86	[53]
MBC@CTS/GCE	0.1-20	20	NR	[54]
TCP/CPE	0.5-10	300	0.59	[55]
MWCNTs/GCE	0.256-3.11	54.9	NR	[56]
Nd_2O_3/*f*-CNF/GCE	0.1-243	4.3	0.142	**This work**

NR – Not reported

3.5. Selectivity, reproducibility, and stability

In order to study the selectivity, the DPV response of CBZ (50 µM) at Nd_2O_3/*f*-CNF/GCE was examined in the presence of various potentially interfering compounds, as shown in **Fig. 5C**. As all other interfering compounds (like pesticides, biological compounds, metal ions, and carbofuran, ascorbic acid, and caffeic acid) have not changed the oxidation peak current of CBZ, the calculated Relative standard deviation (RSD) values are below 3.8%, even when there are excessive amounts of other interfering compounds. According to the obtained results, the modified Nd_2O_3/*f*-CNF/GCE is highly selective for detecting CBZ. A relative error bar is shown in **Fig. 5D**. The CBZ oxidation peak current was not affected by the presence of interfering species; thus, it can be used for monitoring CBZ in real time.

A series of five Nd_2O_3/*f*-CNF/GCEs were prepared and tested for reproducibility in CBZ (50 μM) containing PBS using DPV. The fabricated eight electrodes show similar potential and peak current responses from the obtained DPV curves. The RSD of 3.42% was found for the reproducibility of eight sensors, which shows the excellent reproducibility of the fabricated sensor. The long-term stability of the Nd_2O_3/*f*-CNF/GCE was studied after 20 days of storage in a refrigerator (4°C). DPV performed periodic measurements of the oxidation current response to CBZ (50 μM) at the modified electrode. Despite the long-term stability of the electrode, the peak current value was still 97% of the original value after 22 days. The above results indicate that the modified Nd_2O_3/*f*-CNF/GCE sensor was both reproducible and stable toward the detection of CBZ.

3.6. Real sample analysis

We evaluated the practical feasibility of the proposed CBZ sensor to access practical applications. Analyses of real samples were performed using DPV under similar experimental conditions as those described in **Fig. 5A**. Various water (tap water, pond water, and portable water), soil, and vegetables (brinjals, cabbages, and carrots) samples were used for the real sample analysis. The vegetables were brought from a local market for real sample analysis. Samples of vegetables were cut into small pieces and ground with an electric blender before being analyzed. After collecting the extract, it was centrifuged for 15 minutes at 3000 RPM. The water samples were used directly for real sample analysis; only the pH was adjusted to 7.0 before the analysis. The soil sample was added to the PBS and filtered before analysis for real samples. The DPV test results found that the utilized water, vegetable, and soil samples were CBZ-free after diluting them with PBS. Then, DPV responses of real samples were studied when a known concentration of CBZ was added to the real samples. The standard addition method was used to calculate the recovery, and **Table 2** shows the concentration and recovery results of vegetables, water, and soil samples. The excellent recoveries of CBZ in different vegetables (97.4 – 99.2%), water (96.5 – 99.1%), and soil samples (95.8 – 97.4%) with appropriate relative standard deviation (RSD) were obtained using the fabricated electrode, indicating the excellent practicality of the fabricated sensor. These results confirmed the high accuracy in determining CBZ in the real samples.

Table 2 Determination of CBZ using the Nd_2O_3/*f*-CNF composite modified electrode in different water, vegetable, and soil samples.

Sample	Added (µM)	Found (µM)	Recovery	RSD (%)
Cabbage	5	4.79	98.0	2.1
	10	9.88	98.8	2.3
	20	18.62	97.4	1.3
	30	28.91	98.6	1.5
Brinjal	10	9.89	98.5	2.3
	20	18.99	98.7	3.4
	30	29.81	99.2	1.8
Carrot	10	8.64	97.6	2.3
	20	19.03	98.2	1.9
	30	28.45	98.7	2.6
Soil	10	9.62	96.2	3.4
	20	19.15	95.8	3.9
	30	29.22	97.4	3.7

Drinking water	10	9.91	99.1	1.6
	20	19.78	98.9	1.9
	30	29.65	98.8	1.5
Tap water	10	9.85	98.5	1.9
	20	19.56	97.8	2.4
	30	29.75	99.1	2.1
Pond water	10	9.65	96.5	3.6
	20	19.35	96.8	4.1
	30	29.45	98.2	4.0

4. Conclusions

In conclusion, a straightforward methodology has been used to synthesize the Nd_2O_3/*f*-CNF composite, and its modified electrode was used for the first time for the sensitive and low potential detection of CBZ. Microscopic examinations confirmed the presence of Nd_2O_3 nanoparticles on the surface of *f*-CNF. Also, the other physicochemical studies supported the successful formation of the Nd_2O_3/*f*-CNF composite. In electrochemical studies, it was found that the Nd_2O_3/*f*-CNF composite electrode had a greater surface area and more extraordinary electron transfer ability than Nd_2O_3 and *f*-CNF modified electrodes. The electroanalytical studies determined that the Nd_2O_3/*f*-CNF composite-modified electrode was highly sensitive toward CBZ detection, detecting CBZ at low levels of 4.3 nM with higher sensitivity (0.142 $\mu A \mu M^{-1}$) and providing a more comprehensive linear response range (up to 243 μM). The fabricated composite modified electrode showed excellent selectivity towards CBZ despite the influence of various interfering compounds, including similar insecticides. This excellent recovery of CBZ in water, vegetable, and soil samples confirmed the excellent practicality of the Nd_2O_3 and *f*-CNF-modified electrodes. The synthesized Nd_2O_3/*f*-CNF composite could be applied to environmental remediation in investigated water, vegetable, and soil samples.

Acknowledgments

The authors would like to thank the Khalifa University of Science and Technology and Yeungnam University for providing the necessary support for the study.

References

[1] R. Liu, B. Li, F. Li, V. Dubovyk, Y. Chang, D. Li, K. Ding, Q. Ran, G. Wang, H. Zhao, A novel electrochemical sensor based on β-cyclodextrin functionalized carbon nanosheets@carbon nanotubes for sensitive detection of bactericide carbendazim in apple juice, Food Chem. 384 (2022). https://doi.org/10.1016/j.foodchem.2022.132573.

[2] M.L. Yola, Carbendazim imprinted electrochemical sensor based on CdMoO4/g-C3N4 nanocomposite: Application to fruit juice samples, Chemosphere. 301 (2022) 134766. https://doi.org/10.1016/j.chemosphere.2022.134766.

[3] D. Ilager, S.J. Malode, N.P. Shetti, development of 2D graphene oxide sheets-based voltammetric sensor for electrochemical sensing of fungicide, carbendazim, Chemosphere. 303 (2022) 134919. https://doi.org/10.1016/j.chemosphere.2022.134919.

[4] L. Wei, X. Huang, J. Yang, Y. Wang, K. Huang, L. Xie, F. Yan, L. Luo, C. Jiang, J. Liang, T. Li, Y. Ya, A high performance electrochemical sensor for carbendazim based on porous carbon with intrinsic defects, J. Electroanal. Chem. 915 (2022). https://doi.org/10.1016/j.jelechem.2022.116370.

[5] Y. Li, X. Chen, H. Ren, X. Li, S. Chen, B.C. Ye, A novel electrochemical sensor based on molecularly imprinted polymer-modified C-ZIF67@Ni for highly sensitive and selective determination of carbendazim, Talanta. 237 (2022) 122909. https://doi.org/10.1016/j.talanta.2021.122909.

[6] D. Ilager, N.P. Shetti, Y. Foucaud, M. Badawi, T.M. Aminabhavi, Graphene/g-carbon nitride (GO/g-C3N4) nanohybrids as a sensor material for the detection of methyl parathion and carbendazim, Chemosphere. 292 (2022) 133450. https://doi.org/10.1016/j.chemosphere.2021.133450.

[7] A. Yamuna, T.W. Chen, S.M. Chen, Synthesis and characterizations of iron antimony oxide nanoparticles and its applications in electrochemical detection of carbendazim in apple juice and paddy water samples, Food Chem. 373 (2022) 131569. https://doi.org/10.1016/j.foodchem.2021.131569.

[8] J.F. de Macedo, A.A.C. Alves, M.V.S. Sant'Anna, F.G.C. Cunha, G. de A.R. Oliveira, L.M. Lião, E.M. Sussuchi, Electrochemical determination of carbendazim in grapes and their derivatives by an ionic liquid-modified carbon paste electrode, J. Appl. Electrochem. 52 (2022) 729–742. https://doi.org/10.1007/s10800-021-01665-8.

[9] H. Mahmoudi-Moghaddam, H. Akbari Javar, Z. Garkani-Nejad, Fabrication of platinum-doped NiCo2O4 nanograss modified electrode for determination of carbendazim, Food Chem. 383 (2022) 132398. https://doi.org/10.1016/j.foodchem.2022.132398.

[10] Q. Azizpour Moallem, H. Beitollahi, Electrochemical sensor for simultaneous detection of dopamine and uric acid based on a carbon paste electrode modified with nanostructured Cu-based metal-organic frameworks, Microchem. J. 177 (2022) 107261. https://doi.org/10.1016/j.microc.2022.107261.

[11] R. Elshafey, G.F. Abo-Sobehy, A.E. Radi, Imprinted polypyrrole recognition film @cobalt oxide/electrochemically reduced graphene oxide nanocomposite for carbendazim sensing, J. Appl. Electrochem. 52 (2022) 45–53. https://doi.org/10.1007/s10800-021-01613-6.

[12] L. Wang, S.A. Haruna, W. Ahmad, J. Wu, Q. Chen, Q. Ouyang, Tunable multiplexed fluorescence biosensing platform for simultaneous and selective detection of paraquat and carbendazim pesticides, Food Chem. 388 (2022) 132950. https://doi.org/10.1016/j.foodchem.2022.132950.

[13] N. Nataraj, T.W. Chen, M. Akilarasan, S.M. Chen, A.A. Al-Ghamdi, M.S. Elshikh, Se

substituted 2D-gC3N4 modified disposable screen-printed carbon electrode substrate: A bifunctional nano-catalyst for electrochemical and absorption study of hazardous fungicide, Chemosphere. 302 (2022) 134765. https://doi.org/10.1016/j.chemosphere.2022.134765.

[14] A. Özcan, F. Hamid, A.A. Özcan, Synthesizing of a nanocomposite based on the formation of silver nanoparticles on fumed silica to develop an electrochemical sensor for carbendazim detection, Talanta. 222 (2021). https://doi.org/10.1016/j.talanta.2020.121591.

[15] W. Zhong, F. Gao, J. Zou, S. Liu, M. Li, Y. Gao, Y. Yu, X. Wang, L. Lu, MXene@Ag-based ratiometric electrochemical sensing strategy for effective detection of carbendazim in vegetable samples, Food Chem. 360 (2021) 130006. https://doi.org/10.1016/j.foodchem.2021.130006.

[16] P. Sundaresan, C.C. Fu, S.H. Liu, R.S. Juang, Facile synthesis of chitosan-carbon nanofiber composite supported copper nanoparticles for electrochemical sensing of carbendazim, Colloids Surfaces A Physicochem. Eng. Asp. 625 (2021) 126934. https://doi.org/10.1016/j.colsurfa.2021.126934.

[17] C. Tian, S. Zhang, H. Wang, C. Chen, Z. Han, M. Chen, Y. Zhu, R. Cui, G. Zhang, Three-dimensional nanoporous copper and reduced graphene oxide composites as enhanced sensing platform for electrochemical detection of carbendazim, J. Electroanal. Chem. 847 (2019) 113243. https://doi.org/10.1016/j.jelechem.2019.113243.

[18] Y. Tan, S. Wei, X. Liu, B. Pan, S. Liu, J. Wu, M. Fu, Y. Jia, Y. He, Neodymium oxide (Nd2O3) coupled tubular g-C3N4, an efficient dual-function catalyst for photocatalytic hydrogen production and NO removal, Sci. Total Environ. 773 (2021) 145583. https://doi.org/10.1016/j.scitotenv.2021.145583.

[19] L. Liu, Y. Jia, X. Zhang, S. Chen, S. Wang, J. Zhu, L. Zheng, Z. Chen, L. Huang,

Identification of the function and regulatory network of circ_009773 in DNA damage induced by nanoparticles of neodymium oxide, Toxicol. Vitr. 78 (2022) 105271. https://doi.org/10.1016/j.tiv.2021.105271.

[20] K. Marquez-Mariño, J. Penagos-Llanos, O. García-Beltrán, E. Nagles, J.J. Hurtado, Development of a Novel Electrochemical Sensor Based on a Carbon Paste Electrode Decorated with Nd2O3 for the Simultaneous Detection of Tartrazine and Sunset Yellow, Electroanalysis. 30 (2018) 2760–2767. https://doi.org/10.1002/elan.201800550.

[21] Y. Zhou, Y. Li, P. Han, Y. Dang, M. Zhu, Q. Li, Y. Fu, A novel low-dimensional heteroatom doped Nd2O3 nanostructure for enhanced electrochemical sensing of carbendazim, New J. Chem. 43 (2019) 14009–14019. https://doi.org/10.1039/c9nj02778e.

[22] M. Arunpandian, K. Selvakumar, A. Raja, P. Rajasekaran, M. Thiruppathi, E.R. Nagarajan, S. Arunachalam, Fabrication of novel Nd 2 O 3 /ZnO-GO nanocomposite: An efficient photocatalyst for the degradation of organic pollutants, Colloids Surfaces A Physicochem. Eng. Asp. 567 (2019) 213–227. https://doi.org/10.1016/j.colsurfa.2019.01.058.

[23] V. Arancibia, J. Penagos-Llanos, E. Nagles, O. García-Beltrán, J.J. Hurtado, Development of a microcomposite with single-walled carbon nanotubes and Nd 2 O 3 for determination of paracetamol in pharmaceutical dosage by adsorptive voltammetry, J. Pharm. Anal. 9 (2019) 62–69. https://doi.org/10.1016/j.jpha.2018.11.005.

[24] A. Wahid, A.M. Asiri, M.M. Rahman, One-step facile synthesis of Nd2O3/ZnO nanostructures for an efficient selective 2,4-dinitrophenol sensor probe, Appl. Surf. Sci. 487 (2019) 1253–1261. https://doi.org/10.1016/j.apsusc.2019.05.107.

[25] H. Mohammad Shiri, A. Ehsani, Electrosynthesis of neodymium oxide nanorods and its nanocomposite with conjugated conductive polymer as a hybrid electrode material for

highly capacitive pseudocapacitors, J. Colloid Interface Sci. 495 (2017) 102–110. https://doi.org/10.1016/j.jcis.2017.01.097.

[26] R. Yuvakkumar, S.I. Hong, Nd2O3: novel synthesis and characterization, J. Sol-Gel Sci. Technol. 73 (2015) 511–517. https://doi.org/10.1007/s10971-015-3629-0.

[27] W. Yang, Y. Qi, Y. Ma, X. Li, X. Guo, J. Gao, M. Chen, Synthesis of Nd2O3 nanopowders by sol-gel auto-combustion and their catalytic esterification activity, Mater. Chem. Phys. 84 (2004) 52–57. https://doi.org/10.1016/j.matchemphys.2003.09.042.

[28] S. Đurđić, V. Stanković, F. Vlahović, M. Ognjanović, K. Kalcher, D. Manojlović, J. Mutić, D.M. Stanković, Carboxylated single-wall carbon nanotubes decorated with SiO2 coated-Nd2O3 nanoparticles as an electrochemical sensor for L-DOPA detection, Microchem. J. 168 (2021). https://doi.org/10.1016/j.microc.2021.106416.

[29] J. Tan, X. He, F. Yin, B. Chen, G. Li, X. Liang, H. Yin, Incorporating inactive Nd2O3 into Co/N-doped carbon as bifunctional oxygen electrocatalyst for rechargeable Zn-air battery, Catal. Today. 364 (2021) 67–79. https://doi.org/10.1016/j.cattod.2019.12.018.

[30] Z. Sabir, M. Akhtar, S. Zulfiqar, S. Zafar, P.O. Agboola, S. Haider, S.A. Ragab, M.F. Warsi, I. Shakir, L-Cysteine functionalized Nd2O3/rGO modified glassy carbon electrode: A new sensing strategy for the rapid, sensitive and simultaneous detection of toxic nitrophenol isomers, Synth. Met. 277 (2021) 116774. https://doi.org/10.1016/j.synthmet.2021.116774.

[31] A. Krishnapandi, S.M. Babulal, S.M. Chen, S. Palanisamy, S.C. Kim, M. Chiesa, Surface etched carbon nanofiber companied ytterbium oxide for pinch level detection of fungicides carbendazim, Journal of Environmental Chemical Engineering, 11 (2023) 109059. https://doi.org/10.1016/j.jece.2022.109059.

[32] A.S. Haidyrah, P. Sundaresan, K. Venkatesh, S.K. Ramaraj, B. Thirumalraj, Fabrication of functionalized carbon nanofibers/carbon black composite for electrochemical investigation of antibacterial drug nitrofurantoin, Colloids Surfaces A Physicochem. Eng. Asp. 627 (2021) 127112. https://doi.org/10.1016/j.colsurfa.2021.127112.

[33] M. Sakthivel, S. Ramaraj, S.M. Chen, B. Dinesh, H.V. Ramasamy, Y.S. Lee, Entrapment of bimetallic CoFeSe2 nanosphere on functionalized carbon nanofiber for selective and sensitive electrochemical detection of caffeic acid in wine samples, Anal. Chim. Acta. 1006 (2018) 22–32. https://doi.org/10.1016/j.aca.2017.12.044.

[34] S. Ramki, R. Sukanya, S.M. Chen, M. Sakthivel, Y.T. Ye, Electrochemical detection of toxic anti-scald agent diphenylamine using oxidized carbon nanofiber encapsulated titanium carbide electrocatalyst, J. Hazard. Mater. 368 (2019) 760–770. https://doi.org/10.1016/j.jhazmat.2019.01.110.

[35] D.N. Varun, J.G. Manjunatha, N. Hareesha, S. Sandeep, P. Mallu, C.S. Karthik, N.S. Prinith, N. Sreeharsha, S.M.B. Asdaq, Simple and sensitive electrochemical analysis of riboflavin at functionalized carbon nanofiber modified carbon nanotube sensor, Monatshefte Fur Chemie. 152 (2021) 1183–1191. https://doi.org/10.1007/s00706-021-02839-y.

[36] S. Ramki, R. Sukanya, S.M. Chen, M. Sakthivel, Hierarchical multi-layered molybdenum carbide encapsulated oxidized carbon nanofiber for selective electrochemical detection of antimicrobial agents: Inter-connected path in multi-layered structure for efficient electron transfer, Inorg. Chem. Front. 6 (2019) 1680–1693. https://doi.org/10.1039/c9qi00158a.

[37] S. Ramaraj, S. Mani, S.M. Chen, T. Kokulnathan, B.S. Lou, M.A. Ali, A.A. Hatamleh, F.M.A. Al-Hemaid, Synthesis and application of bismuth ferrite nanosheets supported

functionalized carbon nanofiber for enhanced electrochemical detection of toxic organic compound in water samples, J. Colloid Interface Sci. 514 (2018) 59–69. https://doi.org/10.1016/j.jcis.2017.12.016.

[38] R. Sukanya, M. Sakthivel, S.M. Chen, T.W. Chen, A new type of terbium diselenide nano octagon integrated oxidized carbon nanofiber: An efficient electrode material for electrochemical detection of morin in the food sample, Sensors Actuators, B Chem. 269 (2018) 354–367. https://doi.org/10.1016/j.snb.2018.05.013.

[39] P. Sundaresan, C.C. Fu, S.H. Liu, R.S. Juang, Facile synthesis of chitosan-carbon nanofiber composite supported copper nanoparticles for electrochemical sensing of carbendazim, Colloids Surfaces A Physicochem. Eng. Asp. 625 (2021) 126934. https://doi.org/10.1016/j.colsurfa.2021.126934.

[40] M. Sakthivel, S. Ramaraj, S.M. Chen, B. Dinesh, Synthesis of rose like structured LaCoO3 assisted functionalized carbon nanofiber nanocomposite for efficient electrochemical detection of anti-inflammatory drug 4-aminoantipyrine, Electrochim. Acta. 260 (2018) 571–581. https://doi.org/10.1016/j.electacta.2017.11.122.

[41] V. Muthulakshmi, C. Dhilip Kumar, M. Sundrarajan, Green synthesis of ionic liquid mediated neodymium oxide nanoparticles via Couroupita guianensis abul leaves extract with its biological applications, J. Biomater. Sci. Polym. Ed. 33 (2022) 1063–1082. https://doi.org/10.1080/09205063.2022.2039841.

[42] S. Yang, M. Yang, Q. Liu, X. Wang, H. Fa, Y. Wang, C. Hou, An Ultrasensitive Electrochemical Sensor Based on Multiwalled Carbon Nanotube@Reduced Graphene Oxide Nanoribbon Composite for Simultaneous Determination of Hydroquinone, Catechol and Resorcinol, J. Electrochem. Soc. 166 (2019) B547–B553.

https://doi.org/10.1149/2.0011908jes.

[43] García-Miranda Ferrari A, Foster CW, Kelly PJ, Brownson DAC, Banks CE. Determination of the Electrochemical Area of Screen-Printed Electrochemical Sensing Platforms. Biosensors. 8 (2018) 53. https://doi.org/10.3390/bios8020053.

[44] S. Periyasamy, J. Vinoth Kumar, S.M. Chen, Y. Annamalai, R. Karthik, N. Erumaipatty Rajagounder, Structural Insights on 2D Gadolinium Tungstate Nanoflake: A Promising Electrocatalyst for Sensor and Photocatalyst for the Degradation of Postharvest Fungicide (Carbendazim), ACS Appl. Mater. Interfaces. 11 (2019) 37172–37183. https://doi.org/10.1021/acsami.9b07336.

[45] Y. Dong, L. Yang, L. Zhang, Simultaneous electrochemical detection of benzimidazole fungicides carbendazim and thiabendazole using a novel nanohybrid material-modified electrode, J. Agric. Food Chem. 65 (2017) 727–736. https://doi.org/10.1021/acs.jafc.6b04675.

[46] C.A. Razzino, L.F. Sgobbi, T.C. Canevari, J. Cancino, S.A.S. Machado, Sensitive determination of carbendazim in orange juice by electrode modified with hybrid material, Food Chem. 170 (2015) 360–365. https://doi.org/10.1016/j.foodchem.2014.08.085.

[47] D. Wu, M. Wu, J. Yang, H. Zhang, K. Xie, C. Te Lin, A. Yu, J. Yu, L. Fu, Delaminated Ti3C2Tx (MXene) for electrochemical carbendazim sensing, Mater. Lett. 236 (2019) 412–415. https://doi.org/10.1016/j.matlet.2018.10.150.

[48] R. Cui, D. Xu, X. Xie, Y. Yi, Y. Quan, M. Zhou, J. Gong, Z. Han, G. Zhang, Phosphorus-doped helical carbon nanofibers as enhanced sensing platform for electrochemical detection of carbendazim, Food Chem. 221 (2017) 457–463. https://doi.org/10.1016/j.foodchem.2016.10.094.

[49] C. Tian, S. Zhang, H. Wang, C. Chen, Z. Han, M. Chen, Y. Zhu, R. Cui, G. Zhang, Three-dimensional nanoporous copper and reduced graphene oxide composites as enhanced sensing platform for electrochemical detection of carbendazim, J. Electroanal. Chem. 847 (2019) 113243. https://doi.org/10.1016/j.jelechem.2019.113243.

[50] L. Wei, X. Huang, J. Yang, Y. Wang, K. Huang, L. Xie, F. Yan, L. Luo, C. Jiang, J. Liang, T. Li, Y. Ya, A high performance electrochemical sensor for carbendazim based on porous carbon with intrinsic defects, J. Electroanal. Chem. 915 (2022). https://doi.org/10.1016/j.jelechem.2022.116370.

[51] Y. Zhou, R. Cui, Y. Dang, Y. Li, Y. Zou, Doping controlled oxygen vacancies of ZnWO4 as a novel and effective sensing platform for carbendazim and biomolecule, Sensors Actuators, B Chem. 296 (2019) 126680. https://doi.org/10.1016/j.snb.2019.126680.

[52] D. Ilager, H. Seo, S.S. Kalanur, N.P. Shetti, T.M. Aminabhavi, A novel sensor based on WO3·0.33H2O nanorods modified electrode for the detection and degradation of herbicide, carbendazim, J. Environ. Manage. 279 (2021) 111611. https://doi.org/10.1016/j.jenvman.2020.111611.

[53] A. Yamuna, T.W. Chen, S.M. Chen, T.Y. Jiang, Facile synthesis of single-crystalline Fe-doped copper vanadate nanoparticles for the voltammetric monitoring of lethal hazardous fungicide carbendazim, Microchim. Acta. 188 (2021). https://doi.org/10.1007/s00604-021-04941-8.

[54] R. Liu, Y. Chang, F. Li, V. Dubovyk, D. Li, Q. Ran, H. Zhao, Highly sensitive detection of carbendazim in juices based on mung bean-derived porous carbon@chitosan composite modified electrochemical sensor, Food Chem. 392 (2022) 133301. https://doi.org/10.1016/j.foodchem.2022.133301.

[55] A.M. Ashrafi, J. Dordević, V. Guzsvány, I. Švancara, T. Trtić-Petrović, M. Purenović, K. Vytřas, Trace determination of Carbendazim fungicide using adsorptive stripping voltammetry with a carbon paste electrode containing tricresyl phosphate, Int. J. Electrochem. Sci. 7 (2012) 9717–9731.

[57] W.F. Ribeiro, T.M.G. Selva, I.C. Lopes, E.C.S. Coelho, S.G. Lemos, F. Caxico De Abreu, V. Bernardo Do Nascimento, M.C. Ugulino De Araújo, Electroanalytical determination of carbendazim by square wave adsorptive stripping voltammetry with a multiwalled carbon nanotubes modified electrode, Anal. Methods. 3 (2011) 1202–1206. https://doi.org/10.1039/c0ay00723d.

Credit Author Statement

P.S – Conceptualization, Methodology, Validation, and Writing - Original Draft, Writing - Review & Editing. K.P – Synthesis, Characterization, Electroanalysis & Writing - Original Draft. M.C. – Writing - Review & Editing, Supervision, Resources, Funding acquisition. S-C.K – Resources. The results were discussed by all authors and a final draft was completed by all authors.

Declaration of Interest Statement

Declaration of interests

☒ The authors declare that they have no known competing financial interests or personal relationships that could have appeared to influence the work reported in this paper.

☐The authors declare the following financial interests/personal relationships which may be considered as potential competing interests: